People's Democratic Republic of Algeria
Ministry of Higher Education and Scientific Research

University M'Hamed BOUGARA – Boumerdès

Institute of Electrical and Electronic Engineering

Department of Electronics

Final Year Project Report Presented in Partial Fulfilment of the Requirements of the Degree of

'MASTER'

In **Electrical Engineering**

Option: **Control**

Title:

Automatic Voltage Regulator for Synchronous Generator

Presented By:

- Khalil-Errahmane SARI
- Aimen HADDADI

Supervisor:

Mr. A. Ouadi

Registration Number:...../2018

DEDICATION

To my Family, Friends and Love.

Khalil-Errahmane SARI

To my dear Parents

To my Family and Friends

To the special person in my life, M. Boukraa

Aimen HADDADI

ACKNOWLEDGMENT

First and foremost, we are very thankful to Allah for helping us finish this modest work.

We would like to specially thank our Parents who helped us in every possible way during studies and to express our deep gratitude to our Supervisor Mr. A.Ouadi for his support and guidance throughout the study and realization of this project.

We would like to extend our thanks to everyone who has been a support and to all friends.

THANK YOU.

ABSTRACT

Automatic Voltage Regulator (AVR) is necessary for all power stations producing electricity using synchronous generators (SGs) to ensure constant voltage for the grid connection. This final year report aims to design and implement an AVR based PI-characteristics using Programmable Logic Controller (PLC) for the laboratory 1.5kVA salient pole Lab-volt SG.

Primarily, a mathematical model for the SG is developed. Open circuit, short circuit and three-phase sudden short-circuit tests were realized for several tries in order to accurately identify the different parameters (X_d, X'_d, X''_d, X_q, T'_d and T''_d, etc.) of the SG. Secondly, static self-excitation system is used where a part of the generated voltage is fed-back to the exciter via a semi-controlled rectifier consisting of thyristors and diods. The PLC outputs a control signal to the implemented ramp-comparator strategy firing circuit in order to generate firing pulses to the thyristors. Particle Swarm Optimization (PSO) technique is developed in Matlab to tune the PI-gains.

Lastly, the functionality of the AVR is tested for three different cases where small- and high-valued loads are connected at the SG terminals. The complete system response is shown in terms of voltage and current. Results are discussed validating the use of the AVR implemented.

Table of Contents

List of Figures

List of Tables

GENERAL INTRODUCTION

Power plants have huge importance in electricity generation stations, both in term of production and stability. It is essential that the electricity produced by power plants is stable and of good quality. Most power plants rely on Synchronous generators (SGs) to provide power to the grid. The SGs used are usually of big size and weight, the inertia provided by the rotating mass is significantly huge preventing a lot of disturbances from the grid to affect the rotational speed. Furthermore, the grid connected SGs must be able to maintain a constant level of terminal voltage despite of the disturbances that may cause the deviation of the terminal voltage from its desired value.

The terminal voltage of SGs is monitored and maintained constant by regulating the field current, the automatic voltage regulator (AVR) handles the regulation of that current. The AVR is a device designed to automatically maintain a constant terminal voltage by taking a proper action adjusting the filed current, combined together the AVR and the exciter construct the excitation system.

A typical power conditioner device is an AVR combined with one or more of the following: Surge suppression, short-circuit protection, line noise reduction, phase-to-phase voltage balancing, harmonic filtering, etc. The AVR is mainly used for financial reasons. The deviation from the desired output value may cause malfunction or permanent failure to the supplied electrical equipment that will result in extra costs and downtime. Thus, the AVR is used to primarily maintain voltage within a range of 5% error for safety purposes of the equipment.

The report is structured into five main chapters. Chapter 1 introduces the SG and the development of its mathematical model. For that reason, SG parameters are accurately identified through different identification tests. The tests are then briefly explained and illustrated. Chapter 2 discusses the used excitation system with the AVR based PID- and PI-characteristics. The PID-gains are tuned using the classical Zero/Pole cancelation method in which a simplified model for the SG is developed. The PI-gains on the other hand are tuned using the Particle Swarm Optimization algorithm (PSO). In the 3rd chapter, the complete system is constructed in Matlab/Simulink where simulation is performed. Validation of the developed SG-model and the results of the closed-loop dynamic performance of the controlled system are provided and discussed. The hardware setup of this project is discussed in the 4th chapter. The firing circuit implemented as well as the PLC code developed are explained. Lastly the report is ended up with general conclusion.

CHAPTER 1 : Modelling and Identification of Synch. Generator

1.1 Introduction

A complete synchronous generator (SG) model consists of a combination of a model structure and a set of parameter values. This definition can be broken into two parts. The first part is the construction of the model structure which is the basic form for machine representation. The second part is the evaluation of the model parameters. [1]

The model structure can be formed as lumped-parameter equivalent circuit, transfer function, differential equation representation, etc. On the other hand, the model parameters can be evaluated either based on the manufacturers' data, experimental test results, or some other techniques. [1]

This chapter presents the SG model which is currently used for system studies and analysis. It also represents the tests used in determination of the model parameters and the experimental results of these tests.

1.2 Conventional Model Structure

The schematic of three-phase SG is illustrated in Figure 1.1. SGs consist of two essential elements: field and armature. The field winding carries direct current and produces a magnetic field which induces alternating voltage in the armature windings. [2]

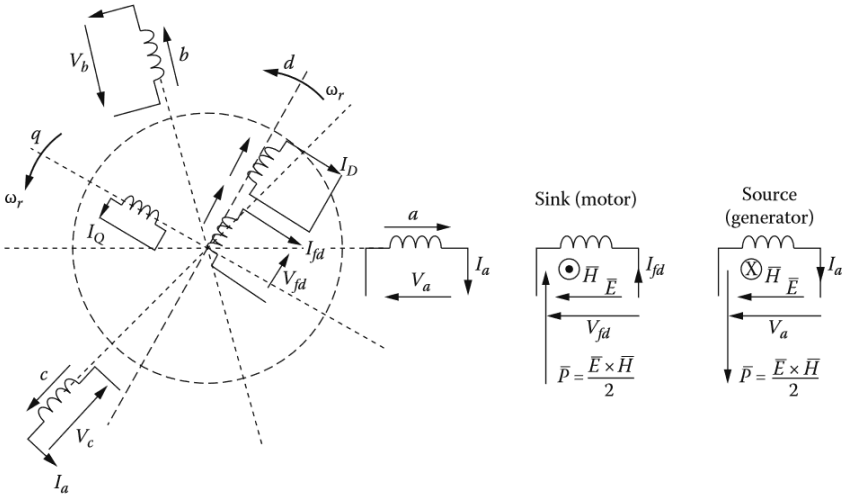

Figure 1-1 Schematic diagram of three-phase synchronous generator.

The three-phase windings of the armature (a, b and c) are distributed 120° electrical degrees apart. The rotor structure has an excitation or field winding and one or more equivalent rotor body windings. The magnetic axis of the machine is defined as the direct-axis (d-axis), and an orthogonal quadratic-axis (q-axis) is located 90° electrical degrees ahead of the d-axis. [2]

Before proceeding in developing model for SG some assumptions are made: [2]

- Magnetic saturation effect, temperature effect and magnetic hysteresis are neglected.
- Stator winding currents are assumed to set up a magneto-motive force (mmf) sinusoidal distributed in space around the air gap. Therefore, the effect of space harmonics in the field distribution is neglected.
- The mmf acting along the d-axis produces a sinusoidal distributed flux wave along that axis. The same for the q- component of the mmf.

1.3 Mathematical Formulation and dq-Model

The model structure is to be formed as a set of equations that are suitable for system studies and analysis. These equation must completely describe the behavior of the SG.

1.3.1 SG in Natural-Reference Frame

By applying Maxwell's equation to the configuration shown in Figure 1.1, the generator phase voltage equations, in natural-reference frame are simply: [2] [3]

$$\begin{aligned} I_A R_s + V_a &= \frac{d\psi_A}{dt} \\ I_B R_s + V_b &= \frac{d\psi_B}{dt} \\ I_C R_s + V_c &= \frac{d\psi_C}{dt} \\ I_f R_f - V_f &= -\frac{d\psi_f}{dt} \\ I_D R_D &= -\frac{d\psi_D}{dt} \\ I_Q R_Q &= -\frac{d\psi_Q}{dt} \end{aligned} \tag{1.1}$$

The flux linkage to current relationship in phase (a) winding at any instant is given by:

$$\psi_A = -L_{AA} I_A - L_{AB} I_B - L_{AC} I_C + L_{Af} I_f + L_{AD} I_D + L_{AQ} I_Q \tag{1.2}$$

Similarly, one can write the flux linkage to current relationships in phases (b) and (c). The flux linking the three-phases of the stator winding is a function of θ. i.e., the angular displacement of the d-axis from phase (a). [2]

Equations (1.1) completely describe the electrical behavior of a SG. However, these equations contain inductance terms which vary with angle θ – rotor position – which in turn varies with time. For that, the machine model was further developed by Park who mathematically transformed the three-phase time-varying stator quantities (voltages, currents and flux linkages) into time-invariant d- and q-axes quantities under steady-state conditions. [1]

The dq-model should express both stator and rotor equations in rotor coordinates, aligned to rotor d- and q-axes because, at least in the absence of magnetic saturation, there is no coupling between the two orthogonal axes. The rotor windings *f*, *D* and *Q* are already aligned along the d- and q-axes. It is only stator equations that have to be transformed to rotor orthogonal coordinates. The transformation from abc- to dq-variables can be written in the following matrix form: [3]

$$\mathrm{P}(\theta)=\frac{2}{3}\begin{pmatrix}\cos(\theta) & \cos(\theta-\frac{2}{3}\pi) & \cos(\theta+\frac{2}{3}\pi)\\ -\sin(\theta) & -\sin(\theta-\frac{2}{3}\pi) & -\sin(\theta-\frac{2}{3}\pi)\end{pmatrix} \tag{1.3}$$

Therefore:

$$\begin{bmatrix}V_d\\V_q\end{bmatrix}=P(\theta)\begin{bmatrix}V_A\\V_B\\V_C\end{bmatrix}$$
$$\begin{bmatrix}I_d\\I_q\end{bmatrix}=P(\theta)\begin{bmatrix}I_A\\I_B\\I_C\end{bmatrix} \tag{1.4}$$
$$\begin{bmatrix}\psi_d\\\psi_q\end{bmatrix}=P(\theta)\begin{bmatrix}\psi_A\\\psi_B\\\psi_C\end{bmatrix}$$

The analysis of SG equations in terms of dq-variables is considerably simpler than in terms of phase quantities, for the following reasons: [2]

- The dynamic performance equations have constant inductances.
- For balanced conditions, zero sequence quantities disappear.
- For balanced steady-state operations, the stator quantities have constant values.
- The parameters associated with d- and q-axes may be directly measured from terminal tests.

The inverse transformation is: [3]

$$P(\theta)^{-1}=\frac{3}{2}P(\theta)^{T} \tag{1.5}$$

The phase currents I_A, I_B and I_C are recovered from I_d and I_q by:

$$\begin{bmatrix}I_A\\I_B\\I_C\end{bmatrix}=P(\theta)^{-1}\begin{bmatrix}I_d\\I_q\end{bmatrix} \tag{1.6}$$

$$\frac{d\theta}{dt}=\omega_r \tag{1.7}$$

Note:

An alternative Park transformation uses $\sqrt{\frac{2}{3}}$ instead of $\frac{2}{3}$ for direct and inverse transform. [3] [2]

The dq-transformation can be seen as representing a SG with orthogonal stator axes fixed magnetically to the rotor d- and q-axes (Figure 1.2). [3]

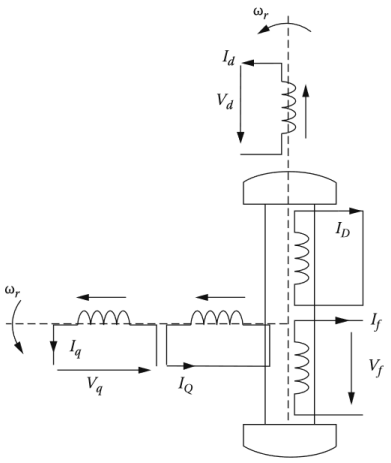

Figure 1-2 The dq-model of synchronous generators.

By applying the dq-transformation the following expressions in terms of transformed components of voltages, flux linkages and currents result: [3]

$$\begin{aligned} I_d R_s + V_d &= \frac{d\psi_d}{dt} - \omega_r \psi_q \\ I_q R_s + V_q &= \frac{d\psi_q}{dt} + \omega_r \psi_d \\ I_f^r R_f^r - V_f^r &= -\frac{d\psi_f^r}{dt} \\ I_D^r R_D^r &= -\frac{d\psi_D^r}{dt} \\ I_Q^r R_Q^r &= -\frac{d\psi_Q^r}{dt} \end{aligned} \tag{1.8}$$

Where:

$$\begin{aligned} \psi_d &= -L_d I_d + M_f I_f^r + M_D I_D^r \\ \psi_q &= -L_q I_q + M_Q I_Q^r \\ \psi_f^r &= (L_{fl}^r + L_{fm}) I_f^r - \frac{3}{2} M_f I_d + \frac{3}{2} M_{fD} I_D^r \\ \psi_D^r &= (L_{Dl}^r + L_{Dm}) I_D^r - \frac{3}{2} M_D I_d + \frac{3}{2} M_{fD} I_f^r \\ \psi_Q^r &= (L_{Ql}^r + L_{Qm}) I_Q^r - \frac{3}{2} M_Q I_q \end{aligned} \tag{1.9}$$

1.3.2 Rotor- to Stator-Reference Frame

Reducing the rotor variable to stator variable is common in order to reduce the number of inductances (Figure 1.3). [3] [5]

$$
\begin{aligned}
I_d R_s + V_d &= \frac{d\psi_d}{dt} - \omega_r \psi_q \\
I_q R_s + V_q &= \frac{d\psi_q}{dt} + \omega_r \psi_d \\
I_f R_f - V_f &= -\frac{d\psi_f}{dt} \\
I_D R_D &= -\frac{d\psi_D}{dt} \\
I_Q R_Q &= -\frac{d\psi_Q}{dt}
\end{aligned}
\tag{1.10}
$$

Flux-current relations with rotor variables reduced to stator would be:

$$
\begin{aligned}
\psi_d &= -L_{sl} I_d + L_{dm}(-I_d + I_D + I_f) \\
\psi_q &= -L_{sl} I_q + L_{qm}(-I_q + I_Q) \\
\psi_f &= L_{fl} I_f + L_{dm}(-I_d + I_D + I_f) \\
\psi_D &= L_{Dl} I_D + L_{dm}(-I_d + I_D + I_f) \\
\psi_Q &= L_{Ql} I_Q + L_{qm}(-I_q + I_Q)
\end{aligned}
\tag{1.11}
$$

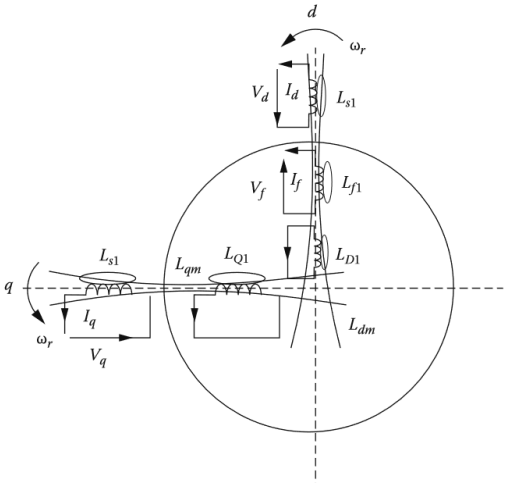

Figure 1-3 The dq-model inductances of synchronous generators.

Comparing equations (1.9) and (1.11), the following definitions of current reduction coefficients are considered valid: [3]

$$
I_f = I_f^r K_f \quad I_D = I_D^r K_D \quad I_Q = I_Q^r K_Q \tag{1.12}
$$

Where:

$$
\begin{cases}
K_f = \dfrac{M_f}{L_{dm}} \\
K_D = \dfrac{M_D}{L_{dm}} \\
K_Q = \dfrac{M_Q}{L_{qm}}
\end{cases}
\tag{1.13}
$$

Using coefficients in equation (1.9) gives:

$$
\psi_f = \psi_f^r . \frac{2}{3} \frac{1}{K_f} \quad \psi_D = \psi_D^r . \frac{2}{3} \frac{1}{K_D} \quad \psi_Q = \psi_Q^r . \frac{2}{3} \frac{1}{K_Q} \tag{1.14}
$$

From equation (1.12) it follows that:

$$L_{fl} = L'_{fl} \cdot \frac{2}{3}\frac{1}{K_f^2} \quad L_{Dl} = L'_{Dl} \cdot \frac{2}{3}\frac{1}{K_D^2} \quad L_{Ql} = L'_{Ql} \cdot \frac{2}{3}\frac{1}{K_Q^2} \tag{1.15}$$

Reducing rotor circuit resistances and field winding voltage to stator quantities results in:

$$R_f = R'_f \cdot \frac{2}{3}\frac{1}{K_f^2} \quad R_D = R'_D \cdot \frac{2}{3}\frac{1}{K_D^2} \quad R_Q = R'_Q \cdot \frac{2}{3}\frac{1}{K_Q^2} \tag{1.16}$$

$$V_f = V'_f \cdot \frac{2}{3}\frac{1}{K_f} \tag{1.17}$$

Note:

When $\sqrt{\frac{2}{3}}$ is used in Park transformation matrix, the reduction coefficients of equation (1.12) must be multiplied by $\sqrt{\frac{3}{2}}$. However, the factor $\frac{2}{3}$ disappears completely from equations (1.14) through (1.17). [3]

1.4 SG Parameters Determination

Till now, two representations of the SG have been developed. The first representation is given by equations (1.8) and (1.9), it requires the determination of the basic parameters (M_f, M_D, M_Q, M_{fD} ...). The second representation is obtained by reducing rotor-variables to stator-variables and is given by equations (1.10) and (1.11).

1.4.1 Experimental Determination of the Laboratory SG Parameters

In order to perform a valid control on the laboratory 1.5kVA salient-pole Lab-Volt SG, parameters of the machine need to be accurately identified. For this purpose, identification tests held in power-lab are performed. Figure 1.4 shows the test bench of the experiment.

Figure 1-4 Test-bench of the experiment.

1.4.1.1 Open-Circuit Test

The test is performed on the SG at no-load to obtain the no-load saturation curve, or simply the open-circuit characteristic (OCC). This last is used graphically to determine the synchronous reactance. During the test, the SG is first run at rated speed of 1500 rpm with no excitation being applied. The filed current is supplied gradually while measuring both terminal voltage and current being supplied to obtain I-V curve. The supplied current is increased until the terminal output voltage reaches the saturation condition. [4]

The obtained curve (Figure 1.5) is a straight line before the saturation zone. The extension of this line for higher values of excitation current gives the air gap line.

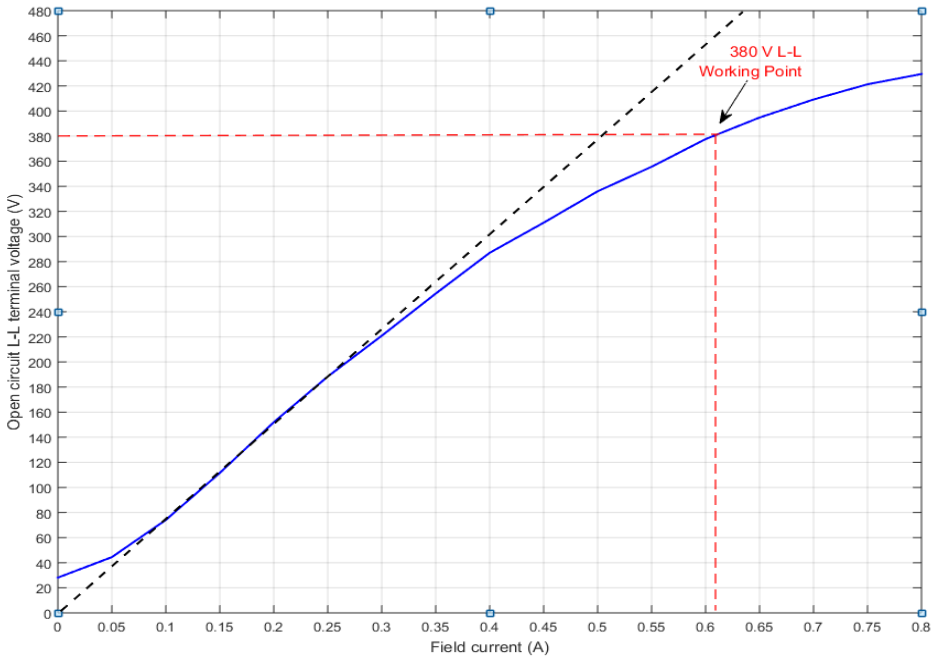

Figure 1-5 Open-circuit characteristics, Lab-Volt SG**.**

1.4.1.2 Sustained Short-Circuit Test

The objective of this test is to obtain the short-circuit saturation curve or simply the short-circuit characteristic (SCC) for the SG. This last is used with the previously obtained curve for the same purpose. It is important to keep track of the excitation current value not to exceed the rated value. The field current might exceed the rated value by only a small tolerance to prevent stator windings damage. [4]

The SG terminals are permanently shorted. The machine is rotating under rated speed of 1500 rpm. The excitation current is injected and increased gradually while measuring the short circuit current flowing in the stator winding. The short-circuit current is plotted versus the

excitation current to obtain the SCC. It is convenient to draw both graphs – open- and short-circuit characteristics – on the same figure (see Figure 1.6).

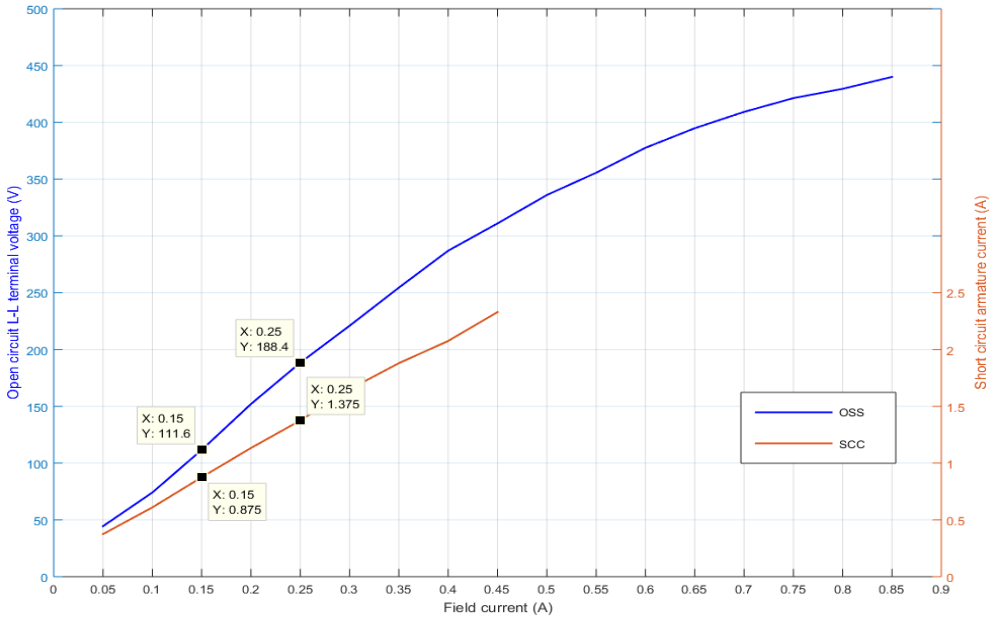

Figure 1-6 Open- and Short-circuit characteristics, Lab-Volt SG.

The d-axis unsaturated impedance $Z_{d\ (unsat)}$ can be obtained as a quotient of voltage on the OCC taken at a point and the short-current armature current on the SCC corresponding to the field current at that very same point [4]. That is:

$$Z_{d(unsat)} = \frac{V_{(L-L)}}{\sqrt{3}I_{SC}} \tag{1.18}$$

The direct-axis unsaturated synchronous reactance $X_{d\ (unsat)}$ is therefore: [4]

$$X_{d(unsat)} = \sqrt{Z_{d(unsat)}^2 - R_s^2} \tag{1.19}$$

Where: R_s is the stator resistance.

1.4.1.3 Slip Test

The aim of the test is to obtain the saliency ratio (X_q/X_d). Using this ratio and the value of X_d obtained from OCC and SCC, X_q is then determined.

The generator during the test is driven at a speed slightly different from the rated speed, about 1% in order to achieve a very small slip. No excitation current is used. A balanced three phase voltage is applied across the SG terminals (about 25% of the rated voltage of the generator) [4]. An oscillogram of the stator voltage and current is recorded (Figure 1.7). Stator current is in grey and is shifted up by 1volt. Whereas, stator voltage is in bleu.

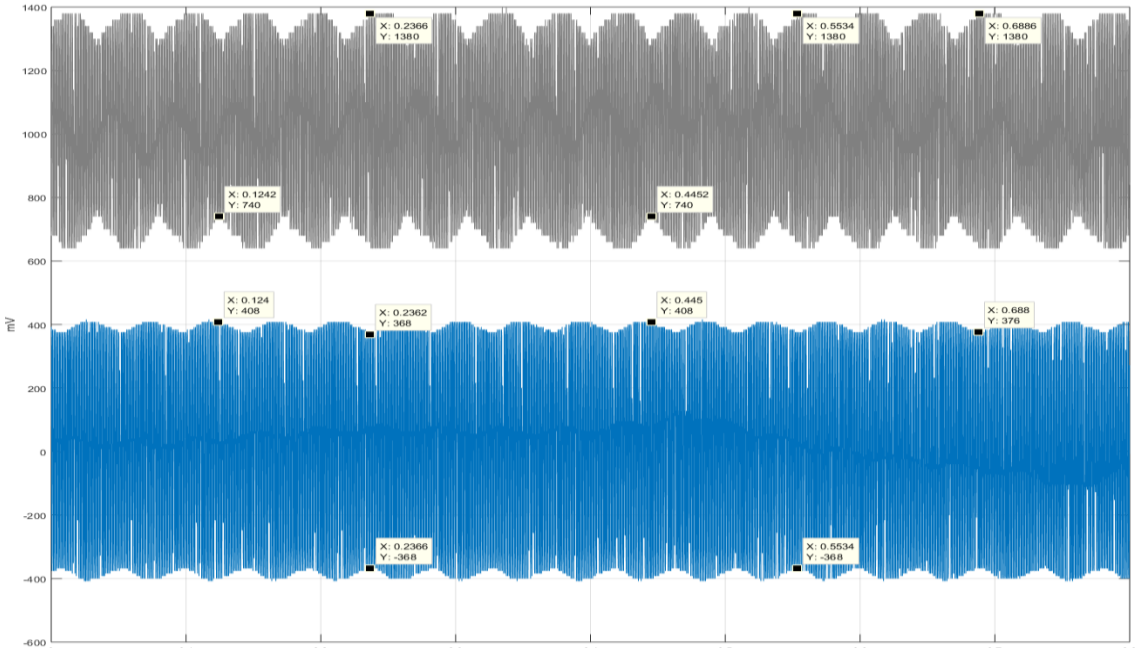

Figure 1-7 Slip test, Lab-Volt SG.

It can be noticed from the figure, at the moment the stator current has its maximum the stator voltage has its minimum and vice-versa. Using the graph, and after calibrating the current as well as the voltage transducers, the following calculations can be made: [4]

$$X_{\mathrm{d(slip)}} = \frac{V_{t(L-L)\max}}{\sqrt{3} I_{\min}}$$
$$X_{q(\mathrm{slip})} = \frac{V_{t(L-L)\min}}{\sqrt{3} I_{\max}} \tag{1.20}$$

The saliency ratio is: [4]

$$\left[\frac{X_q}{X_d}\right]_{slip} = \frac{X_{q(\mathrm{slip})}}{X_{d(\mathrm{slip})}} \tag{1.21}$$

Finally, X_q is obtained: [4]

$$X_q = X_d \left[\frac{X_q}{X_d}\right]_{slip} \tag{1.22}$$

1.4.1.4 Sudden Three-Phase Short Circuit Test

The goal of the test is to visualize the behavior of the SG during dynamic and electric transients when a sudden three phase short circuit is applied. Many of the transient and sub-transient parameters can be computed from a suitable oscillogram recorded during the three phase short circuit. The test aim to calculate direct-axis transient X_d' and sub-transient reactance X_d".

The SG is driven at the rated speed with no load, and is excited so that the terminal voltage is at the rated value. The next step is to apply a sudden three phase short-circuit. The current at each phase is recorded with time [4]. A typical current waveform is shown below (Figure 1.8).

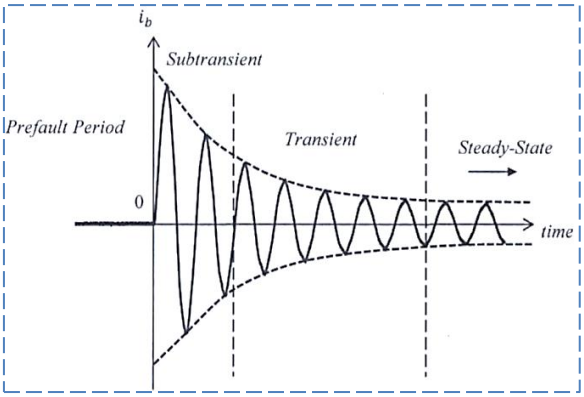

Figure 1-8 Typical phase short-circuit current.

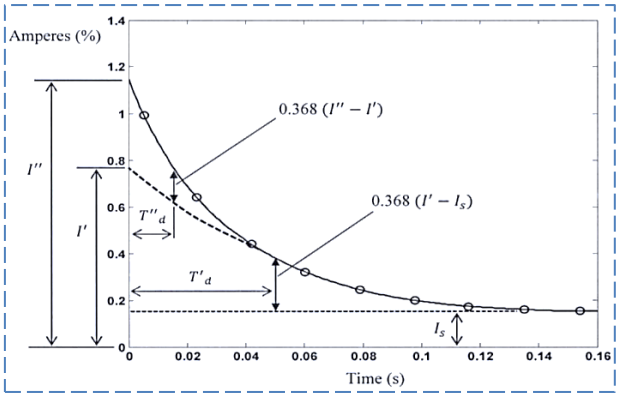

Figure 1-9 Polynomial curve fitting for positive peaks of the phase short-circuit current.

The rms amplitude of the total ac component of the short circuit current in one phase can be expressed as: [4]

$$I_{sc}(t) = \left(I'' - I'\right)e^{\frac{-t}{T_d''}} + \left(I' - I_s\right)e^{\frac{-t}{T_d'}} + I_s \tag{1.23}$$

$$I_{sc}(t) = E_o\left[\left(\frac{1}{X_d''} - \frac{1}{X_d'}\right)e^{\frac{-t}{T_d''}} + \left(\frac{1}{X_d'} - \frac{1}{X_d}\right)e^{\frac{-t}{T_d'}} + \frac{1}{X_d}\right] \tag{1.24}$$

Where E_o is the rms line-to-neutral open circuit pre-fault terminal voltage.

By extrapolating the sub-transient and transient current envelope back to zero-time or the time of the short-circuit occurrence, the sub-transient and transient current components can be evaluated. The value of X_d' and X_d'' can now be calculated: [4]

$$\begin{cases} X_d' = \dfrac{E_o}{I'} \\ X_d'' = \dfrac{E_o}{I''} \end{cases} \tag{1.25}$$

The time constants T_d' and T_d'' as well as the transient and sub-transient short-circuit currents I' and I'' respectively can now be determined (Figure 1.9).

Results of the identification tests performed are finally summarized (Table 1.1).

Nominal power	S_n	*1.5 kVA*
Nominal rms line-to-neutral voltage	U_n	*220 v*
Frequency	f_n	*50 Hz*
Stator resistance	R_s	*2.2* Ω
Rotor resistance	R_f	*127* Ω
Direct-axis synchronous reactance (unsaturated)	X_d	*75.443* Ω
Quadrature-axis synchronous reactance (unsaturated)	X_q	*46.556* Ω
Direct-axis open-circuit time constant	T_{do}'	*0.235 s*
Direct-axis transient reactance	X_d'	*10.309* Ω
Direct-axis transient time constant	T_d'	*0.0776 s*
Direct-axis sub-transient reactance	X_d''	*8.5298* Ω
Quadrature-axis sub-transient reactance	X_q''	*5.2637* Ω
Direct-axis sub-transient time constant	T_d''	*0.0147 s*

Table 1-1 1.5kVA salient-pole Lab-Volt SG parameters.

In order to simulate the model obtained, leakage inductances must be determined. The parameters of the SG used in this work are obtained in terms of reactances and time constants (Table 1.1). For that, mathematical relations between these parameters and leakage inductances need to be found.

Mathematical relations can be written in the following forms (Table 1.2): [2] [5]

$X = Lw_r$	$X_d' = X_{sl} + \frac{X_{dm}X_{fl}}{X_{dm} + X_{fl}}$	$T_d' = \frac{1}{\omega_r R_f}(X_{fl} + \frac{X_{sl}X_{dm}}{X_{sl} + X_{dm}})$	$T_{do}' = \frac{X_{dm} + X_{fl}}{\omega_r R_f}$
$X_d = X_{sl} + X_{dm}$	$X_d'' = X_{sl} + \frac{X_{fl}X_{Dl}}{X_{fl} + X_{Dl}}$	$T_d'' = \frac{1}{\omega_r R_D}(X_{Dl} + \frac{X_{sl}X_{fl}}{X_{sl} + X_{fl}})$	$T_{do}'' = \frac{1}{\omega_r R_D}(X_{Dl} + \frac{X_{fl}X_{dm}}{X_{fl} + X_{dm}})$
$X_q = X_{sl} + X_{qm}$	$X_q'' = X_{sl} + \frac{X_{qm}X_{Ql}}{X_{qm} + X_{Ql}}$	$T_q'' = \frac{1}{\omega_r R_Q}(X_{Ql} + \frac{X_{sl}X_{qm}}{X_{sl} + X_{qm}})$	$T_{qo}'' = \frac{X_{qm} + X_{Ql}}{\omega_r R_Q}$

Table 1-2 Mathematical relations between time constants and reactances.

Based on the expressions above, the following result: [5]

$X_{dm} = \sqrt{T_{do}' w_r R_f (X_d - X_d')}$ $X_{sl} = X_d - X_{dm}$ $X_{qm} = X_q - X_{sl}$	$X_{Dl} = \frac{(X_d'' - X_{sl})X_{fl}}{X_{fl} + X_{sl} - X_d''}$	$R_D = \frac{1}{\omega_r T_{do}''}(X_{Dl} + \frac{X_{dm}X_{fl}}{X_{dm} + X_{fl}})$	$T_{do}'' = \frac{X_d'}{X_d''}T_d''$
$X_{fl} = T_{do}' w_r R_f - X_{dm}$	$X_{Ql} = \frac{(X_q'' - X_{sl})X_{qm}}{X_{qm} + X_{sl} - X_q''}$	$R_Q = \frac{X_{qm} + X_{Ql}}{\omega_r T_{qo}''}$	$T_{qo}'' = \frac{X_q}{X_q''}T_q''$

Table 1-3 Parameters of the mathematical model.

1.5 Determination of Reduction Coefficients K_f, K_D and K_Q

The coefficients K_f, K_D and K_Q used in the reduction of rotor-variables to the stator may be calculated through analytical or numerical methods, but they may be also measured. [3] [5]

The reduction factor of the excitation K_f can be obtained directly from steady-state short-circuit test by taking the average value of the reduction factors obtained at different values of field current. (see figures 1.10 – 1.11). [5]

$$K_f = \frac{I_f}{\sqrt{3}Isc} \tag{1.26}$$

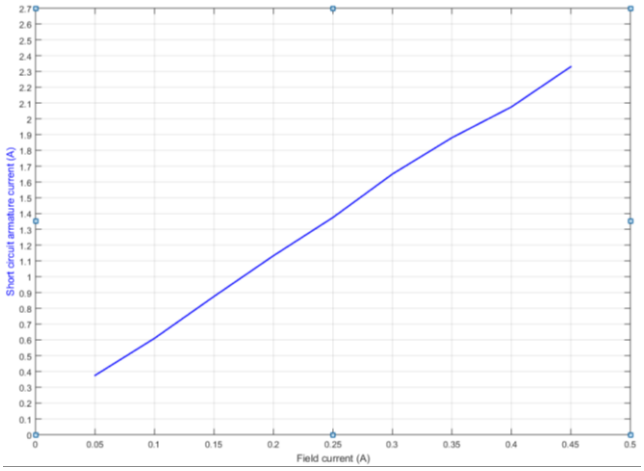

Figure 1-10 Short-circuit characteristics, Lab-Volt SG.

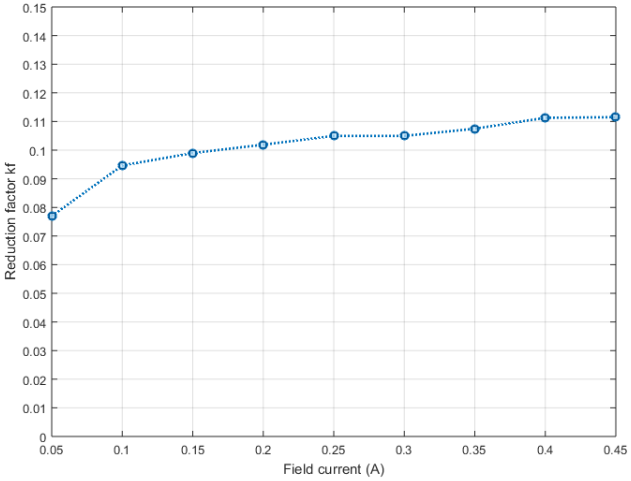

Figure 1-11 Excitation reduction coef. K_f versus field current.

The dampers reduction coefficients K_D and K_Q on the other hand are essentially needed to measure damper currents I_D and I_Q. However, these current are not measured practically and since it is possible to see the machine behavior without using these coefficient there is an infinite solution to them.

CHAPTER 2 : Excitation System with Automatic Voltage Regulator

2.1 Introduction

Synchronous Generators (SGs) with field windings require DC-supplies to excite them, and as they are constant speedy machines for constant frequency supply, the output voltage depends radically on the excitation current. The control of excitation current to maintain constant voltage at the SG output terminals starts with the control of the exciter (Figure 2.1).

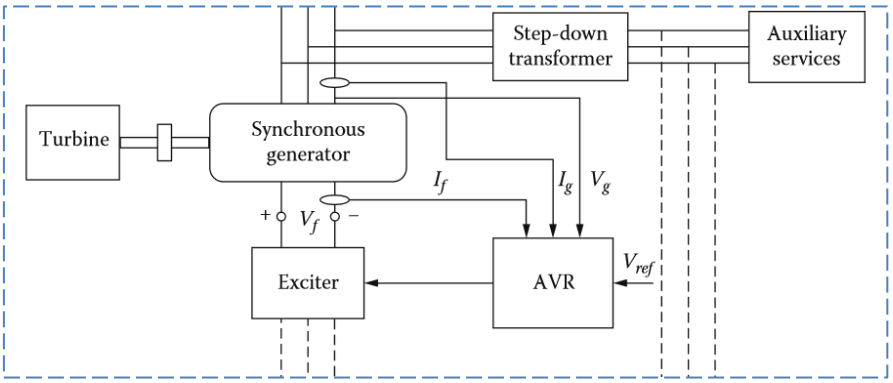

Figure 2-1 Structure of excitation system with AVR.

The performance requirements of the excitation system are determined by considering the SG. Along supplying and automatically adjusting the field current, the excitation system plays an important role in protection and stability of the machine, it must respond rapidly to disturbances to enhance system robustness.

In this chapter, the structure and the working principle of the excitation system used in this work are presented. The functionality of each part of the excitation system along with the automatic voltage regulator (AVR) are discussed. The controller gains are tuned using the zero/pole cancelation and the particle swarm optimization (PSO) methods.

2.2 Excitation System

Excitation systems are in fact the power supply that deliver power to the SG field winding. They have taken many forms over the years and can be classified into three types: DC-, AC- and Static-Exciters. The design and types of exciters have been developed through time to meet requirements. The DC- and AC-exciters contain an electric generator coupled on the main shaft and have low power electronics control of their excitation current. The static exciters however take energy from an AC source and convert it into a DC-controlled power which is fed to the field winding of the SG through slip rings and brushes. [3]

Modern electric power plants gave way to static exciters (power electronics) where controlled rectifiers supply directly the excitation of the SG. This is due to its fast and good response in voltage and power control and due to its satisfactory steady state stability condition.

Among the Static exciter configurations, consider the configuration used in this work (Figure 2.2) where the AC source is the SG output terminals. [3]

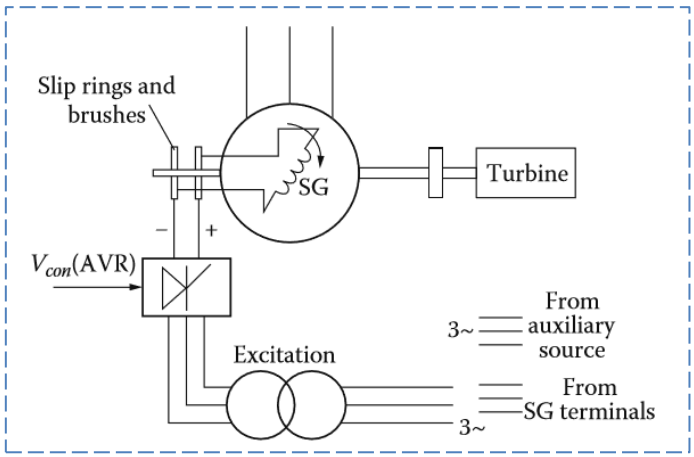

Figure 2-2 Structure of static excitation system.

2.2.1 Working Principle of the Excitation System Used

Excitation power is supplied through a transformer from the main generator terminals. Commonly known as Transformer-fed excitation system (Figure 2.3). Power electronics is used to supply the excitation current to the field winding of the machine. The generator terminal voltage is measured and fed to the programmable logic controller (PLC). The PLC regulates the generator output voltage by controlling the firing pulses of the thyristors.

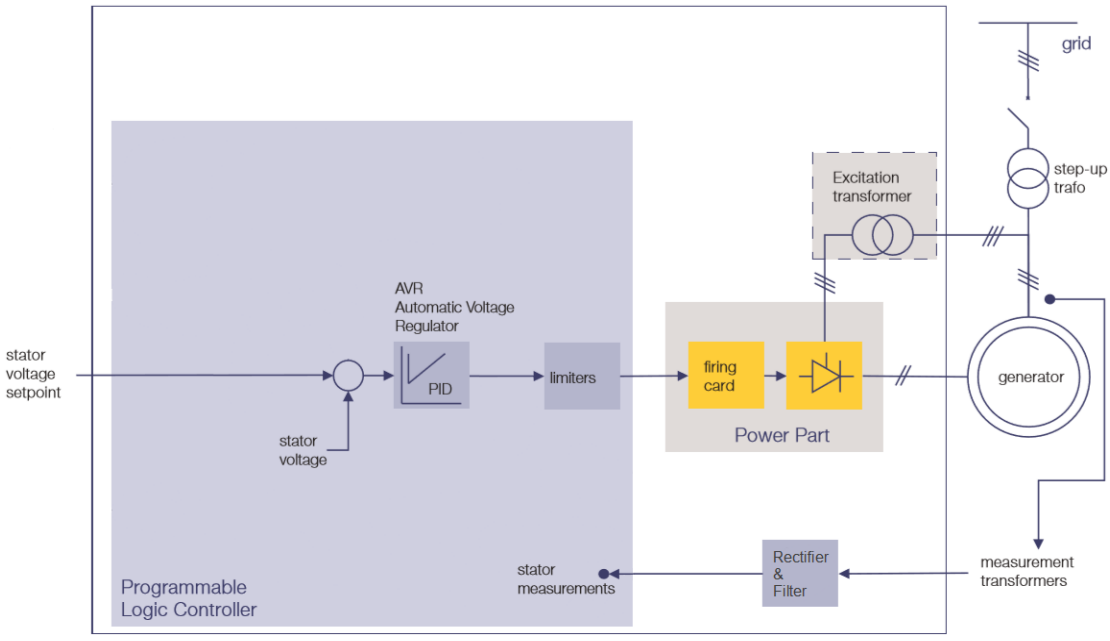

Figure 2-3 Scheme of the excitation system used.

2.2.2 Functionality and System Components

The complete (global) system components and their functionalities can be summarized in the following four points:

- **Excitation Power and Excitation Transformer**

The excitation power is derived from the machine terminals and is conducted via power-electronics into the field winding of the SG. The purpose of the excitation transformer is to adapt the power supply to the converter and to isolate the field winding from the power supply.

The secondary voltage is dimensioned according to the required ceiling voltage, whereas, the current rating of the transformer is determined by the maximum field current of the SG.

- **Power Circuit**

A semi-controlled rectifier consisting of thyristors and diodes is to provide power to the field winding and is controlled by the PLC via the firing circuit that converts the output control DC voltage signal from the PLC to firing pulses (details can be seen in section 4.1).

The power circuit is provided with protection against voltage transients. This is achieved by RC snubber circuits.

- **Measurement System**

Measurement of stator voltage is done by means of measurement transformer followed by a full wave rectifier and a precision peak detector. (See Appendix I)

- **Automatic Voltage Regulator**

The AVR control algorithm is to provide closed-loop control of the SG output voltage by keeping it constant. Also, the AVR is required to maintain the stability of the generator in steady-state, as well as during transient disturbances and shall cover all control functions needed for the excitation system.

2.3 AVR based PID-Characteristics

The AVR senses the error in SG terminals voltage with respect to the voltage set-point, and causes corrective action – proportional, integral and derivative – to take place. The output is then a control voltage $V_{con\ (AVR)}$. [6]

The transfer function of a PID-controller is:

$$G_{PID}(s) = K_P(1 + \frac{1}{sT_I} + sT_D) = K_P(\frac{1 + sT_I + s^2T_IT_D}{sT_I}) \qquad (2.1)$$

With: K_P – proportional gain, T_I – integral constant time, T_D – derivative constant time.

For fast and good response in voltage control and rejecting disturbances, the PID-controller need to be tuned. Selecting PID-parameters is called controller tuning, two methods are to be applied in this work: The conventional Zero/Pole cancelation method and the Particle Swarm Optimization (PSO) method.

Although the AVR is to be implemented digitally, the design of the PID-controller may be done as if it were continuous, because the sampling frequency is more than 20 times the damped frequency of the closed-loop system. [3]

2.3.1 Zero/Pole Cancelation in Tuning the PID-Controller

The AVR output depends only on the output voltage of the generator. The linearized model of an AVR system with PID-controller is described below (Figure 2.4). The excitation system is of the type IEEE-ST1A. [2]

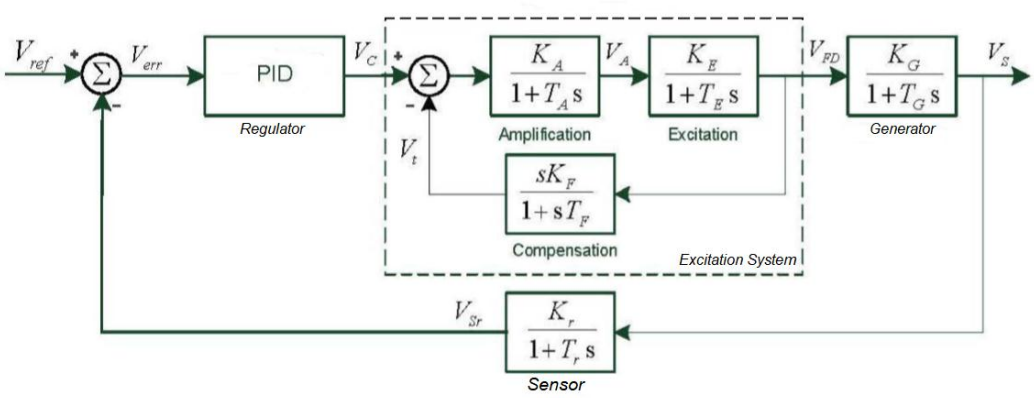

Figure 2-4 Regulation principle of SG terminal voltage.

Simplifying the global system above results in:

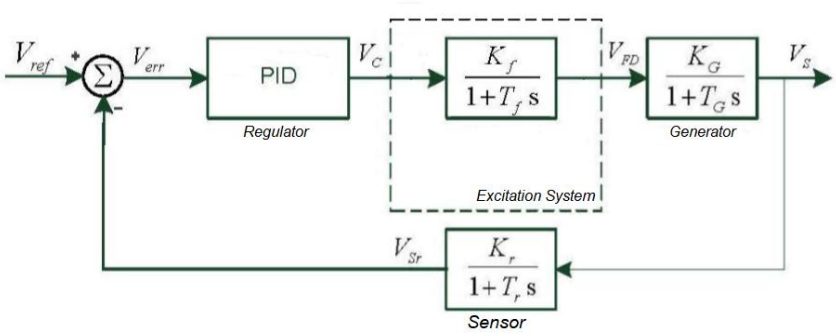

Figure 2-5 Simplified model of the voltage regulation principle.

The control signal is given by:

$$V_c = K_P\left[e(t) + \frac{1}{T_I}e(t)dt + T_D\frac{de(t)}{dt}\right] \tag{2.2}$$

Where: *e(t)* is the error voltage.

The transfer function of *(excitation system + generator)* is then obtained:

$$G_{EG}(s) = \frac{K_f K_G}{(1+sT_f)(1+sT_G)} = \frac{K_{EG}}{1+s(T_f+T_G)+s^2 T_f T_G} \tag{2.3}$$

After applying Zero/Pole cancelation eliminating the poles of equation (2.3) by the zeros of equation (2.1):

$$\begin{cases} T_I = T_f + T_G \\ T_D = \dfrac{T_f T_G}{T_f + T_G} \end{cases} \tag{2.4}$$

The forward-path transfer function is then reduced to:

$$\begin{aligned} G_{FP}(s) &= \frac{K_{FP}}{sT_I} \\ K_{FP} &= K_P K_f K_G \end{aligned} \tag{2.5}$$

Let *H(s)* be the sensor transfer function:

$$H(s) = \frac{K_r}{1+sT_r} \tag{2.6}$$

The closed-loop transfer function of a negative feedback system is given by:

$$G_{cl} = \frac{G_{FP}(s)H(s)}{1+G_{FP}(s)H(s)} \tag{2.7}$$

Replacing equation (2.5) and (2.6) into equation (2.7) yields to the global system transfer function:

$$\begin{aligned} G_{cl} &= \frac{\left(\dfrac{K_{FP}}{sT_I}\right)\left(\dfrac{K_r}{1+sT_r}\right)}{1+\left(\dfrac{K_{FP}}{sT_I}\right)\left(\dfrac{K_r}{1+sT_r}\right)} \\ &= \frac{1}{1+\left(\dfrac{sT_I}{K_{FP}}\right)\left(\dfrac{1+sT_r}{K_r}\right)} \\ &= \frac{1}{1+s\left(\dfrac{T_I}{K_{FP}K_r}\right)+s^2\left(\dfrac{T_I T_r}{K_{FP}K_r}\right)} \end{aligned} \tag{2.8}$$

Given the transfer function of a second order system:

$$G(s) = \frac{1}{1+s\left(\dfrac{2\xi}{\omega_n}\right)+s^2\left(\dfrac{1}{\omega_n^2}\right)} \tag{2.9}$$

From equations (2.8) and (2.9) and by identification:

$$\begin{cases} \dfrac{T_I}{K_{FP}K_r} = \dfrac{2\xi}{\omega_n} \\ \dfrac{T_I T_r}{K_{FP}K_r} = \dfrac{1}{\omega_n^2} \end{cases} \tag{2.10}$$

$$\omega_n = \frac{2\xi K_{FP}K_r}{T_I} \tag{2.11}$$

$$K_{FP} = \frac{T_I T_r \omega_n^2}{K_r} \tag{2.12}$$

Replacing equation (2.11) into equation (2.12) yields:

$$K_{FP} = \frac{T_I}{4 T_r K_r \xi^2} \tag{2.13}$$

Finally, from equations (2.4), (2.5) and (2.13) we deduce the gains:

$$\begin{cases} K_P = \dfrac{\left(T_f + T_G\right) T_r \omega_n^2}{K_r K_f K_G} \\ or \\ K_P = \dfrac{\left(T_f + T_G\right)}{4 K_f K_G T_r K_r \xi^2} \end{cases} \qquad K_I = \frac{1}{T_f + T_G} \quad \& \quad K_D = \frac{T_f T_G}{T_f + T_G} \tag{2.14}$$

2.3.1.1 Calculation of Different TFs Parameters

- **The Simplified SG TF**

The simplified transfer function describing the SG is of the form:

$$G(s) = \frac{K_G}{(1 + sT_G)} \tag{2.15}$$

Finding K_G and T_G can be done as follows:

$$\begin{cases} G(s) = K_G \dfrac{1 + sT_{kd}}{\left(1 + sT_{do}^{'}\right)\left(1 + sT_{do}^{''}\right)} \\ K_G = \dfrac{x_{md}}{r_f} \\ T_{do}^{'} = \dfrac{x_{md} + x_f}{r_f} \end{cases} \tag{2.16}$$

With:

$x_{md} \; x_f \rightarrow T_G = T_{d\grave{o}}^{'} \; \dfrac{x_f}{r_f}$

T_{kd} and $T_{do}^{''}$ are neglected. [7]

- **The Amplifier TF**

The relationship between the generator output voltage and the AC-DC converter output voltage is given by: [7]

$$V_{S_{DC}} = 0.9 V_{S_{ab\_eff}} \cos(\alpha) \tag{2.17}$$

$$\begin{cases} V_f = 0.9 V_2 \cos(\alpha) = 0.9 K_e V_G \cos(\alpha) \\ V_c = V_{tb} \cos(\alpha) = K_{tb} V_G \cos(\alpha) \end{cases} \tag{2.18}$$

Where:

$$\begin{cases} K_e = \dfrac{V_2}{V_G} \\ K_{tb} = \dfrac{V_{tb}}{V_G} \end{cases} \tag{2.19}$$

V_f: is the voltage applied to the field winding.

V_2: is the rms value of the secondary winding of the excitation transformer.

V_{tb}: is the maximum generator output voltage.

The amplifier gain can be calculated then:

$$V_f = 0.9 K_e V_G \frac{V_c}{K_{tb} V_G} = K_f V_c \tag{2.20}$$

$$K_f = 0.9 \frac{K_e}{K_{tb}} \tag{2.21}$$

Finally, the time constant T_f is given by:

$$T_f = \frac{T}{2} \tag{2.22}$$

2.3.1.2 Disadvantages of Conventional Tuning Methods

The disadvantages of classical tuning methods are:

- Difficulty to deal with non-linear process.
- Inadequate dynamics of closed loop response.
- Excessive number of rules to set the gains.

It is difficult to find suitable PID-parameters using classical mathematical approaches. For that, alternative and modern heuristics optimization techniques such as Particle Swarm Optimization PSO, Genetic Algorithm GA, Bat algorithm and others have been given much attention due to their ability to find global solution in PID tuning.

2.3.2 Particle Swarm Optimization Technique

PSO is an evolutionary computation algorithm which is founded upon the principles of biological evolution and is inspired by the study and investigation of swarm patterns occurring in nature. [9]

PSO was first introduced by Eberhart and Kennedy in 1995 [10] [11], many researchers have expanded on the original idea with alterations ranging from minor parameter adjustments to complete reworking of the algorithm.

PSO is used to explore the search space of a given problem to find the settings or parameters required to maximize or minimize an objective function. It is found to be robust in

solving problems featuring nonlinearity and non-differentiability, multiple optima, and high dimensionality problems. [9]

2.3.2.1 PSO Concept

PSO uses a number of particles (or agents) flying in the multidimensional space in order to locate a good optimum. Through the flight, each particle which is a candidate solution adjusts it flying based on two reasoning capabilities: its memory of its own best local position visited so far (Pbest), and knowledge of the global best (Gbest). At first, the particles are distributed along the search space randomly, then each particle velocity and position is updated each iteration. Using an objective function to calculate the fitness, the algorithm decides which particle is closer to the solution and saves the best local position and the global best position for each particle. [9]

PSO algorithm can be summarized by the following steps:

- Randomly initialize the particles positions.

For each iteration, the following steps are repeated:

- Calculate the fitness for each particle.
- Evaluate the local best for each particle.
- Evaluate the global best.
- Update velocity and Update position.

2.3.2.2 PSO Parameters

The parameters used in the algorithm affect its performance differently. Some parameters have small effects while other have significant effects. Each set of parameters might be valid for a problem but not for another. The choice of parameters depends on the problem in hand and the time the user wants to spend solving it. [12]

The main parameters that should be considered are:

- **Swarm Size**

Swarm size or the number of agents (n) in the swarm. A large number generates larger parts covered in the search space, this means less iterations are needed, but also more computation by iteration is needed. Most implementations use $n \in [20, 60]$.

- **Iteration Number**

The number the algorithm updates the position of particles (number of steps). A large number may cause additional needless computations while a low number may stop the algorithm before hitting its target.

- **Personal-best and Global-best**

The algorithm uses a memory to save for each particle its best position visited so far. For each iteration, the actual position is compared with the personal best, if the cost function is decreasing, the actual position is a better fit and the personal best is updated to be the actual. If not, the particle keeps the previous personal best. The global best on the other hand is updated each iteration by taking the minimum of *Pbest*.

$$Pbest_i^{t+1} = \begin{cases} Pbest_i^t & if \quad f(x_i^{t+1}) > fbest_i^t \\ xbest_i^{t+1} & if \quad fbest_i^t \geq f(x_i^{t+1}) \end{cases}$$
$$Gbest^t = Min(Pbest_1^t, Pbest_2^t, Pbest_3^t, \ldots, Pbest_n^t) \tag{2.23}$$

- **Velocity and Its Updating Methods**

The velocity is the rate of change in the particle's position. Represented as a vector and calculated over each iteration as follow:

$$v_i^{t+1} = v_i^t + c_1 r_1 * (Pbest_i^t - x_i^t) + c_2 r_2 * (Gbest^t - x_i^t) \tag{2.24}$$

c_1, c_2: are two positive constants.

r_1, r_2: are two positive randomly generated numbers less than 1.

- **Inertia Weight Method:**

Shi and Eberhart introduced the damping factor ω to further control the velocity by the following equation:

$$v_i^{t+1} = \omega^t v_i^t + c_1 r_1 * (Pbest_i^t - x_i^t) + c_2 r_2 * (Gbest^t - x_i^t)$$
$$\omega^t = \omega_{\max} - \frac{\omega_{\max} - \omega_{\min}}{t_{\max}} t \tag{2.25}$$

Usually, ω takes a maximum value of 0.9 at the first iteration and decreases to a minimum value of 0.4 in the last one which causes the decrease of velocity of particles going from an exploratory search to exploitative search. [13]

- **Constriction Factor Method:**

Clerc and kenedy introduced a new parameter X constriction factor, this last controls the exploration and exploitation tradeoff to ensure convergence behavior. [14]

The velocity updated using this method is:

$$v_i^{t+1} = X\left\{v_i^t + c_1 r_1 * (Pbest_i^t - x_i^t) + c_2 r_2 * (Gbest^t - x_i^t)\right\}$$
$$X = \frac{2}{\left|2 - \sqrt{\varphi^2 - 4\varphi} - \varphi\right|} \tag{2.26}$$
$$\varphi = c_1 + c_2$$

Studies shows that: to guarantee quick convergence, ϕ must be greater than 4, otherwise the system will be slow and might diverge. [14]

- **Position Update**

After the particles being randomly initiated, each iteration the position of each particle is updated according to the equation:

$$x_i^{t+1} = x_i^t + v_i^{t+1} \tag{2.27}$$

- **Stopping Rule**

The algorithm is terminated after a specified number of iteration, or once the fitness of particles are small enough, which means close enough to the solution.

2.3.2.3 PSO in Tuning the PI-Controller

The flowchart of the code implemented in this work is shown next. The velocity update is set to be inertia weight based. The performance criteria used in designing the PI-controller is the Integrated of Time weight Square Error (ITSE).

$$ITSE = \int t.e(t)^2 \tag{2.28}$$

The advantage of ITSE over other integral performance criteria, say Integrated Square Error (ISE) and Integrated Absolute Error (IAE) is that ITSE can overcome the disadvantage these last two may face. ISE and IAE minimizations can result in response with small overshoot but a long settling time because they weight all error equally independent of time.

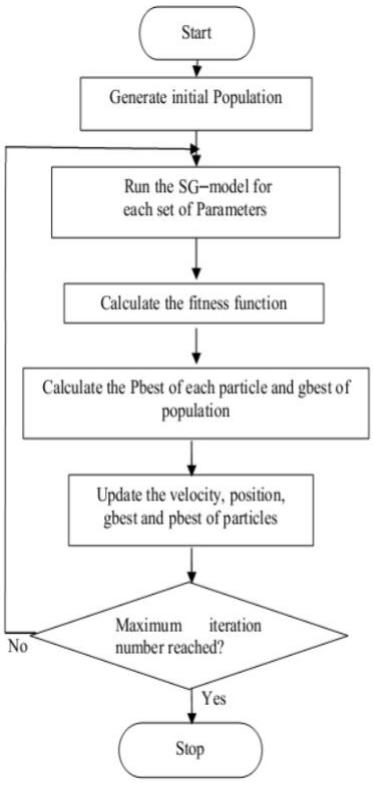

Figure 2-6 Flowchart for the PSO based PI-controller.

2.4 Thyristor Firing Circuit

A common arrangement of a firing circuit scheme is shown below (Figure 2.7). Gating pulses from the triggering circuit for each thyristor should be applied at specific instant of time to make the control possible. Hence, synchronization is required. In other words, the firing angle α is to be measured from the instant V_a of the SG is zero and going positive for T1. Similarly for T2, α is to be measured from the instant V_a of the SG is zero and going negative. It is noted that each thyristor is conducting for 180° only. [8]

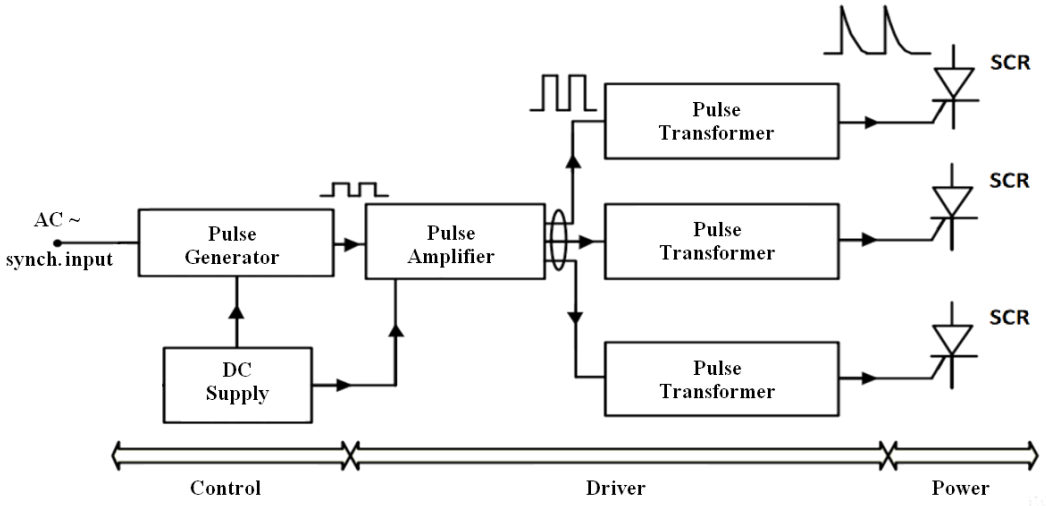

Figure 2-7 General layout of the firing circuit scheme for thyristors.

The expression for the output voltage is then a function of parameter α as it is described by equation (2.17).

2.4.1 Ramp-Comparator Strategy Control

One method of firing angle control is the ramp-comparator strategy where a ramp signal is generated in synchronism with the SG terminal phase voltage V_a. The control voltage $V_{con\ (AVR)}$ is compared to the synchronized ramp generated giving out voltage pulses (figure 2.8). However, these pulses might not be able to turn-on the thyristors. Therefore, a driver circuit involving pulse amplifier for amplification and pulse transformer for isolating the low voltage circuit from the high voltage circuit is needed. [8]

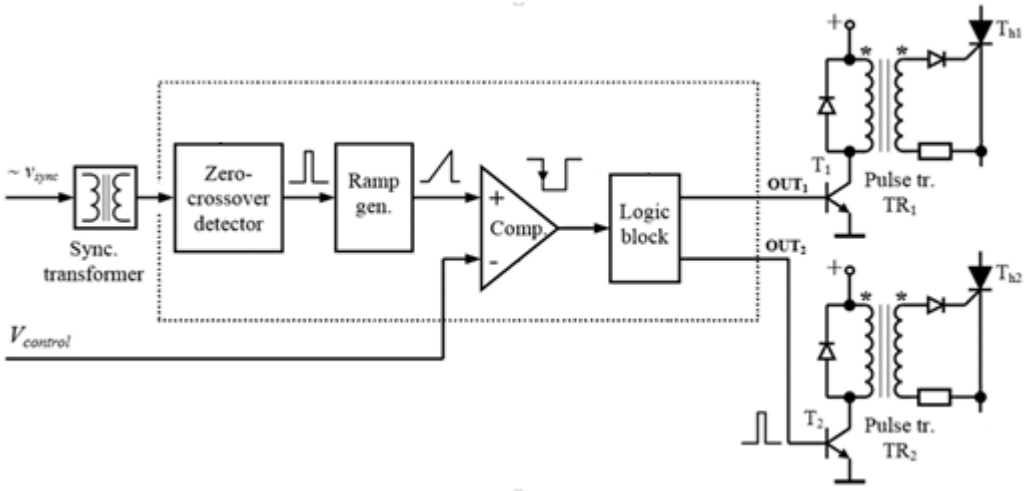

Figure 2-8 Firing circuit scheme for the thyristors.

CHAPTER 3 : Simulation and Results

3.1 Introduction

Before proceeding into implementing this project, simulation of the complete system behavior is needed. Using Matlab/Simulink and with the help of SimPowerSystem library provided, the previously explained system is then implemented. (See Appendix II)

Validation of the SG-model and of the automatic voltage regulator is presented in this chapter.

3.2 SG Simulation Model

The simulation of the model obtained in the 2nd chapter is performed using Matlab/Simulink. The system of equations (1.10) and (1.11) can be written as:

$$\begin{cases} V_d = -R_s I_d + (\mathrm{L}_{sl} + \mathrm{L}_{qm})\omega_r I_q - L_{qm}\omega_r I_Q - (\mathrm{L}_{sl} + \mathrm{L}_{dm})\dfrac{dI_d}{dt} + L_{dm}\dfrac{dI_f}{dt} + L_{dm}\dfrac{dI_D}{dt} \\ V_q = -R_s I_q - (\mathrm{L}_{sl} + \mathrm{L}_{dm})\omega_r I_d + L_{dm}\omega_r I_f + L_{dm}\omega_r I_D - (\mathrm{L}_{sl} + \mathrm{L}_{qm})\dfrac{dI_q}{dt} + L_{dm}\dfrac{dI_Q}{dt} \\ V_f = R_f I_f + (\mathrm{L}_{fl} + \mathrm{L}_{dm})\omega_r I_d - L_{dm}\dfrac{dI_d}{dt} + L_{dm}\dfrac{dI_D}{dt} \\ 0 = R_D I_D + (\mathrm{L}_{Dl} + \mathrm{L}_{dm})\dfrac{dI_D}{dt} + L_{dm}\dfrac{dI_f}{dt} - L_{dm}\dfrac{dI_d}{dt} \\ 0 = R_Q I_Q + (\mathrm{L}_{Ql} + \mathrm{L}_{qm})\dfrac{dI_Q}{dt} - L_{qm}\dfrac{dI_q}{dt} \end{cases} \tag{3.1}$$

In matrix form:

$$\begin{bmatrix} V_d \\ V_q \\ V_f \\ 0 \\ 0 \end{bmatrix} = Z \begin{bmatrix} I_d \\ I_q \\ I_f \\ I_D \\ I_Q \end{bmatrix} + L\frac{d}{dt}\begin{bmatrix} I_d \\ I_q \\ I_f \\ I_D \\ I_Q \end{bmatrix} \tag{3.2}$$

With:

$$Z = \begin{pmatrix} -R_s & (\mathrm{L}_{sl} + \mathrm{L}_{qm})\omega_r & 0 & 0 & -\mathrm{L}_{qm}\omega_r \\ -(\mathrm{L}_{sl} + \mathrm{L}_{dm})\omega_r & -R_s & \mathrm{L}_{dm}\omega_r & \mathrm{L}_{dm}\omega_r & 0 \\ 0 & 0 & R_f & 0 & 0 \\ 0 & 0 & 0 & R_D & 0 \\ 0 & 0 & 0 & 0 & R_Q \end{pmatrix} \tag{3.3}$$

$$L = \begin{pmatrix} -(\mathrm{L}_{sl} + \mathrm{L}_{dm}) & 0 & \mathrm{L}_{dm} & \mathrm{L}_{dm} & 0 \\ 0 & -(\mathrm{L}_{sl} + \mathrm{L}_{qm}) & 0 & 0 & \mathrm{L}_{qm} \\ -\mathrm{L}_{dm} & 0 & (\mathrm{L}_{fl} + \mathrm{L}_{dm}) & \mathrm{L}_{dm} & 0 \\ -\mathrm{L}_{dm} & 0 & \mathrm{L}_{dm} & (\mathrm{L}_{Dl} + \mathrm{L}_{dm}) & 0 \\ 0 & -\mathrm{L}_{qm} & 0 & 0 & (\mathrm{L}_{Ql} + \mathrm{L}_{dm}) \end{pmatrix} \tag{3.4}$$

It is possible then to write the system in state-space (SS) representation:

$$\begin{cases} \dfrac{dX}{dt} = AX + BU \\ Y = CX \end{cases} \tag{3.5}$$

With:

$A = -L^{-1}Z,\ B = L^{-1},\ U = \left[V_d, V_q, V_f, 0, 0\right]^T \quad X = \left[I_d, I_q, I_f, I_D, I_Q\right]^T$ n

In order to create terminals *A*, *B* and *C* and to generate and measure three-phase voltage, star-connected resistances r_{exc} of 10^4 Ω are put. The implementation scheme of this model in Matlab-Simulink software is shown below (Figure 3.1). [5]

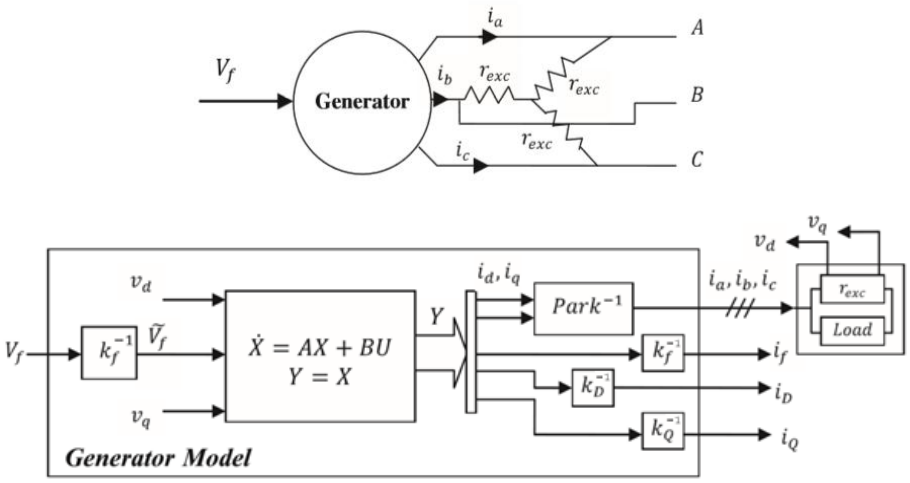

Figure 3-1 Synchronous generator representation in Simulink.

Note:

ω_r can be considered as a constant parameter in matrix Z since speed variations is neglected.

3.3 Validation of the SG-Model Obtained

To check the fitness of the model developed, a three-phase short-circuit is applied across the SG, it represents a high load impact on the machine.

The three-phase short-circuit is applied at 55% rated voltage. The field current as well as the armature current obtained by experimental tests and those obtained by simulation are plotted on same graphs (see Figures 3.2 – 3.3).

Sudden three-phase short-circuit, at 55% rated voltage.

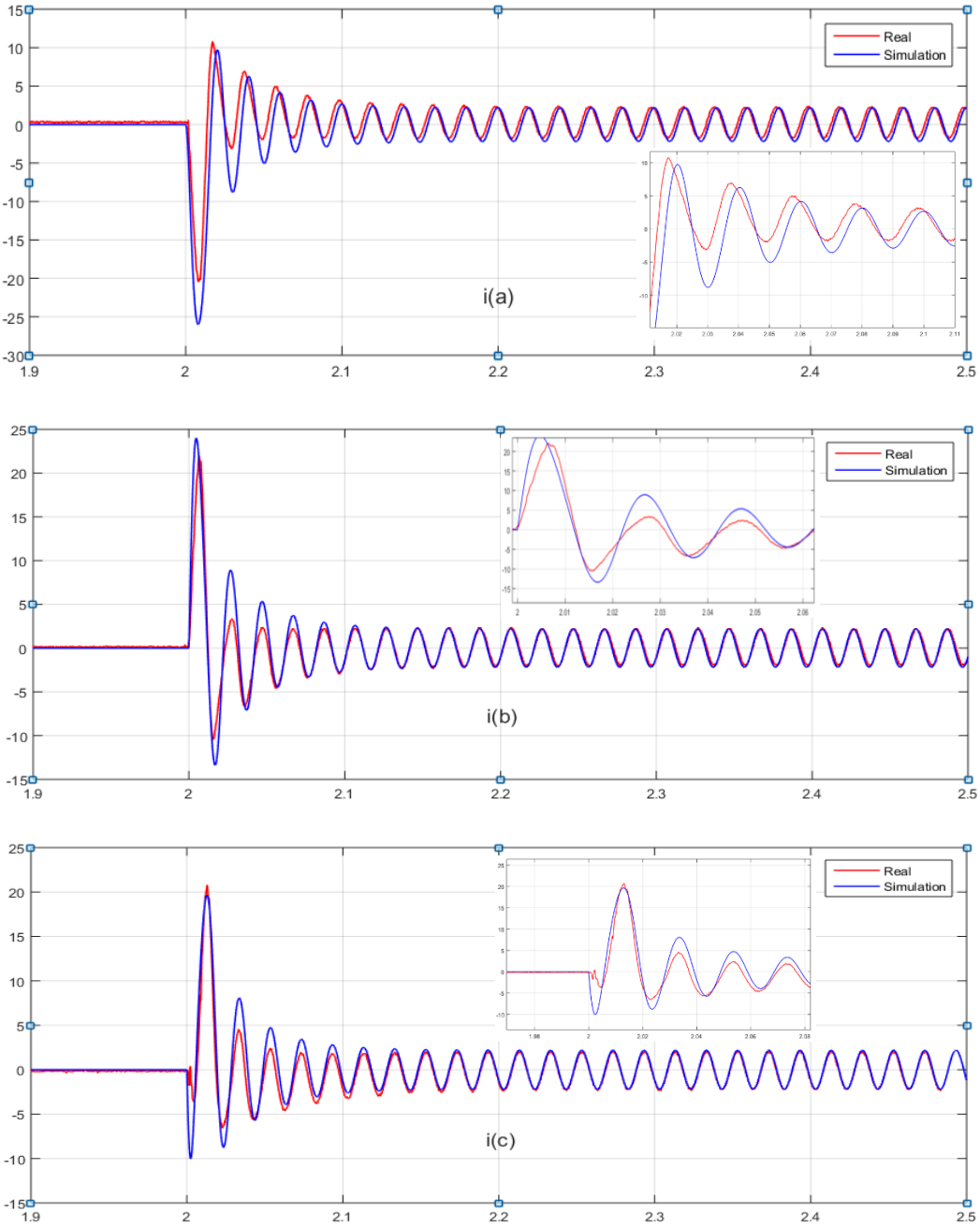

Figure 3-2 Real and simulation armature current.

Sudden three-phase short-circuit, at 55% rated voltage.

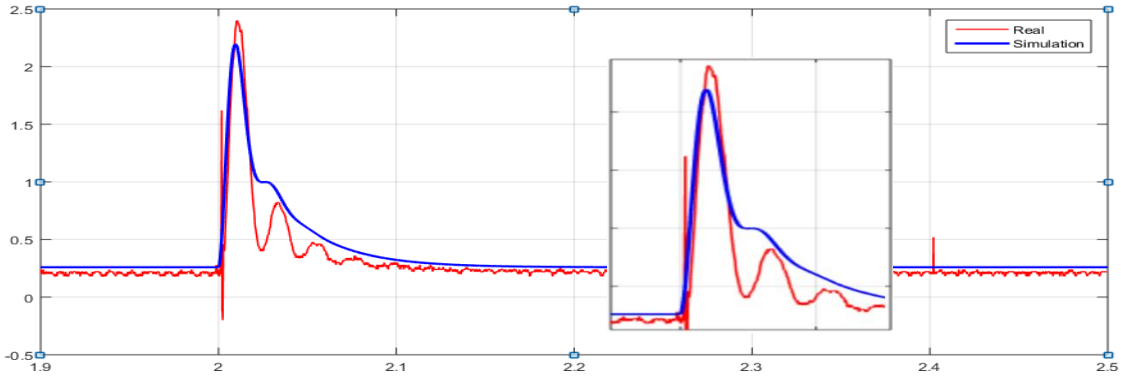

Figure 3-3 Real and simulation armature current.

As it is shown above, the real and simulation current quantities have approximately the same waveforms. The calculated quantities have very similar shapes to the real ones. The difference is due to the approximations made obtaining the model – the neglected effects of saturation and hysteresis – and due to measurement errors performing the identification tests.

3.4 System Closed-Loop Performance

The purpose of this work is to maintain constant voltage at the Lab-Volt SG terminals regardless to the variation of loads connected to it. For that reason, the complete system is implemented in Simulink and is considered the closest possible to the real one (see Appendix-1). The response of the system to loads variation – resistive loads are modelled as pure resistances in series with small valued inductances, whereas, inductive loads are modelled as pure inductances in series to small valued resistances – is to be discussed.

The SG is first run at no load in its rated conditions. At *t=1s*, a load is connected to the machine terminals. A controller of unity gain is used first. The phase-to-neutral rms voltage and three-phase rms currents are shown below.

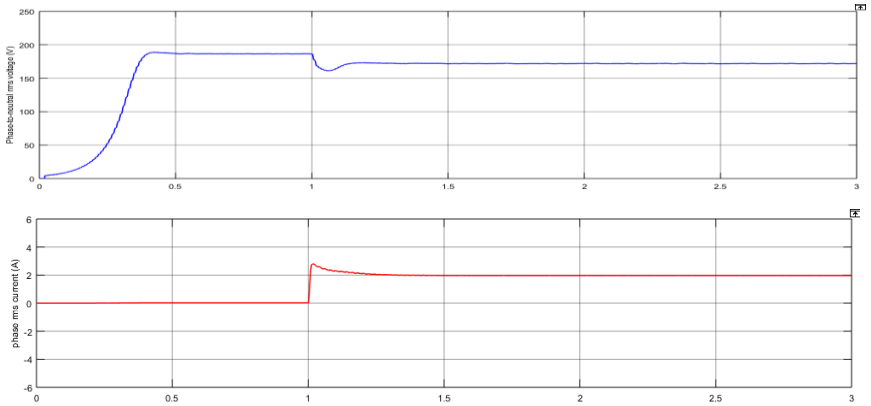

Figure 3-4 Phase-to-neutral rms voltage and three-phase rms current.

It can be seen that a steady state error voltage is presented before connecting the load. However, after load connection a decay of voltage is captured, this is due to load current rise (see figure 3.4).

Note:

The system with unity control is not able to reach the reference voltage and to reject the effect of connecting loads. That is, loads are considered disturbance to the system.

For the system to give better performance in closed-loop, PI-controller is introduced.

3.4.1 PSO Tuning Results

The PSO algorithm was coded in Matlab. And by using the Simulink SG-model, the algorithm simulates the output of the SG for each particle's position each iteration in order to calculate the error and the dynamic characteristics of the system. (See Figure 2.6)

The PSO parameters are set to be:

Number of variables (Dimension of the problem)	*2*
c_1	*2*
c_2	*2*
Velocity updating method	*Inertia weight*
Wmax	*0.9*
Wmin	*0.4*
Lower bound (position)	*[0.1 0.5]*
Upper bound (position)	*[3 3]*
Fitness function	*ITSE*

Table 3-1 PSO parameters settings.

Running the PSO algorithm for several tries and for different parameters of population size and number of iterations, the results obtained are displayed and are in terms of best solution for K_P and K_I along with PSO convergence characteristics graphs. (See Figure 3.5)

1st Try:

Population Size:

20

Number or Iteration:

10

Best Solution:

$$\begin{cases} K_P = 0.9857 \\ K_I = 0.6029 \end{cases}$$

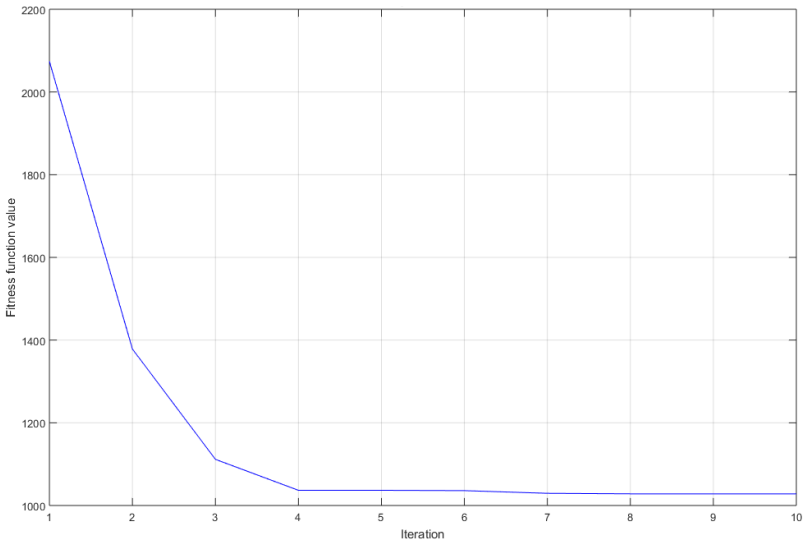

2nd Try:

Population Size:

30

Number or Iteration:

20

Best Solution:

$$\begin{cases} K_P = 0.9899 \\ K_I = 0.6035 \end{cases}$$

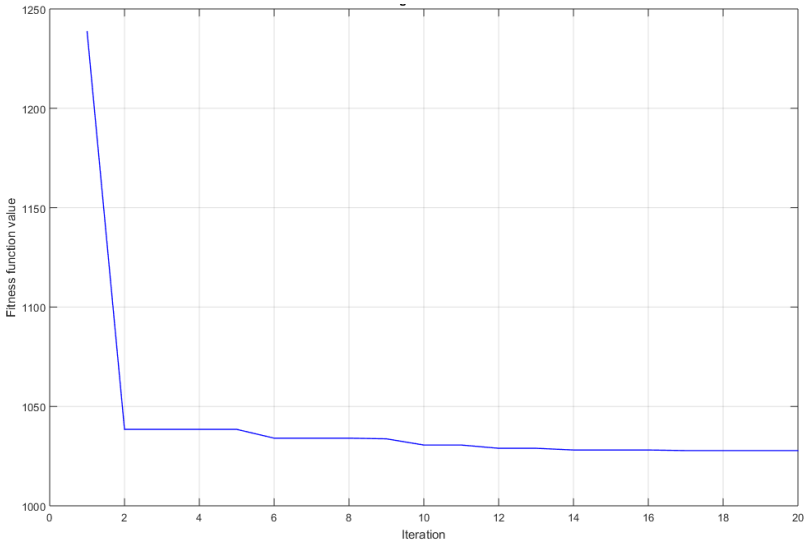

3rd Try:

Population Size:

50

Number or Iteration:

40

Best Solution:

$$\begin{cases} K_P = 0.9915 \\ K_I = 0.5958 \end{cases}$$

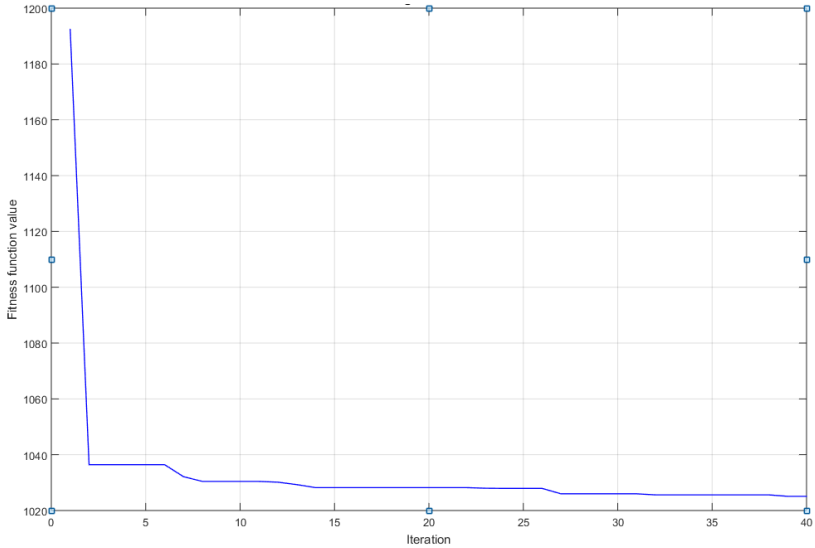

Figure 3-5 PSO convergence characteristics and best solutions.

3.5 Application on the SG

Setting the PI-parameters obtained above (Table 3.2). The AVR based PI-controller's functionality is tested for different valued loads connecting at different times of operation. The machine is set to work at its rated values, at *t=1s* a load is suddenly connected. Table 3.3 summarizes the different types and values of loads to be connected to the SG terminals.

	P (Watt)	*Q (VAR)*	*pf*
1st case	270	130.7	0.9
2nd case	675	326.92	0.9
3rd case	90	286.19	0.3
4th case	270 then +90	130.7 then +286.19	0.3

Table 3-2 Used loads during disturbance tests.

In order to better see the response of the system, the rms phase-to-neutral voltage is presented. The system response is to be discussed next.

Before introducing disturbance to the system – load connection – the SG is set working at rated conditions, that is, the phase-to-neutral rms voltage is regulated to *220 volts*.

At *t=1s*, a *270Watts and 130.7VARs* load is suddenly connected (1st case). As it is seen in figure 3.5 (a) and 3.5 (c) a drop in voltage followed by a rise in current is observed. The AVR senses this drop causing corrective actions to take place giving rise to field voltage, hence, field current (Figure 3.5 b). It is also remarkable that the load has small influence on the SG terminal voltage and that the performance of the PI-controller before and after applying disturbance is considered valid.

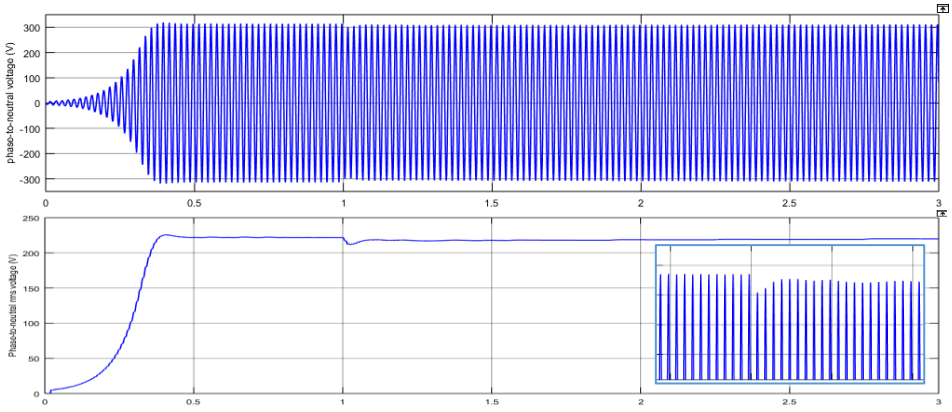

Figure 3-6 Phase-to-neutral and phase-to-neutral rms output voltage. 1st case.

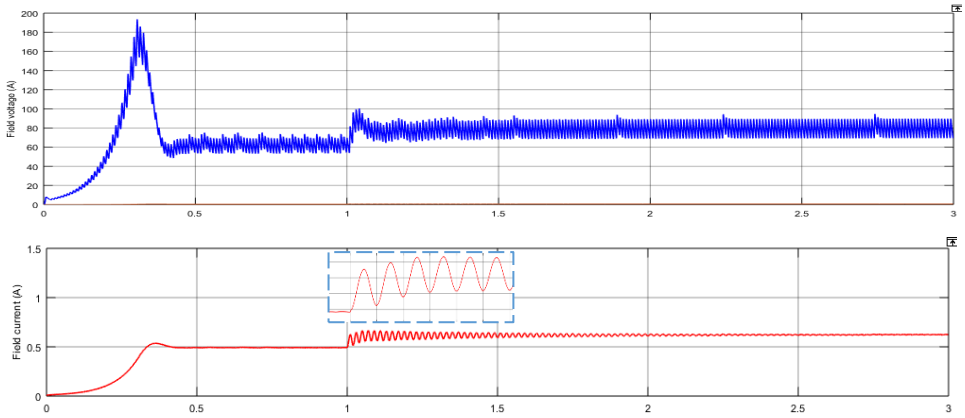

Figure 3-7 Field voltage and field current. 1st case.

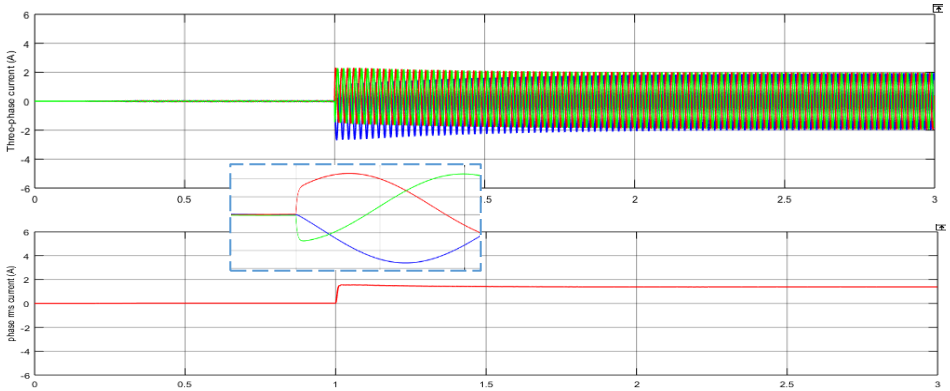

Figure 3-8 Three-phase current and single-phase rms current. 1st case.

The 2nd case disturbance is done by connecting a higher valued load to the SG terminals. A load that consumes half of the nominal apparent power with a 0.9 power factor *(675Watts and 326.92VARs)*. The influence of this 2nd case is greater comparing to the 1st one. The field current rises considerably to compensate the drop in voltage (Figure 3.6 b). Also, the system takes longer time to reach stability again.

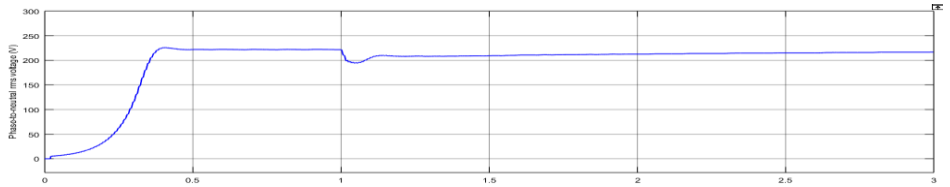

Figure 3-9 Phase-to-neutral rms output voltage. 2nd case.

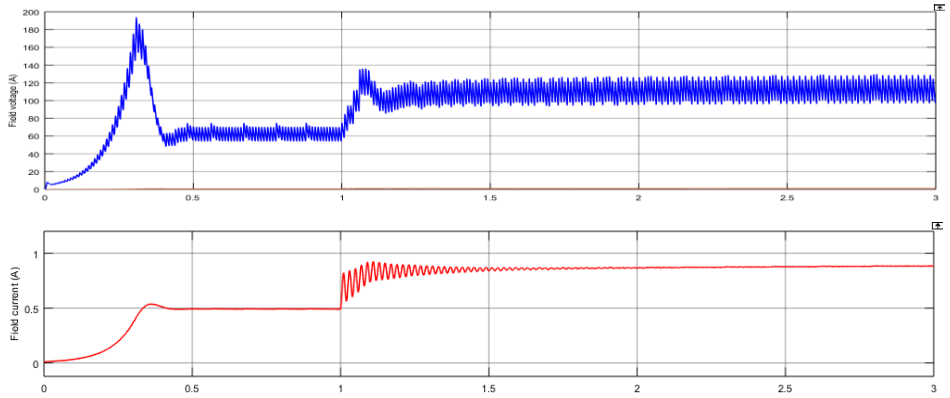

Figure 3-10 Field voltage and field current. 2nd case.

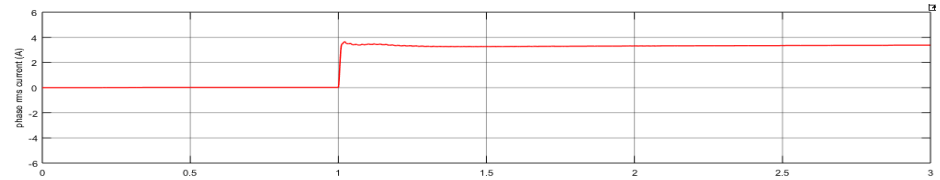

Figure 3-11 Single-phase rms current. 2nd case.

The 3rd case disturbance on the other hand deals with a 0.3 power factor load. Even though the load is of another type (reactive) the AVR tends to reject its effect on the system.

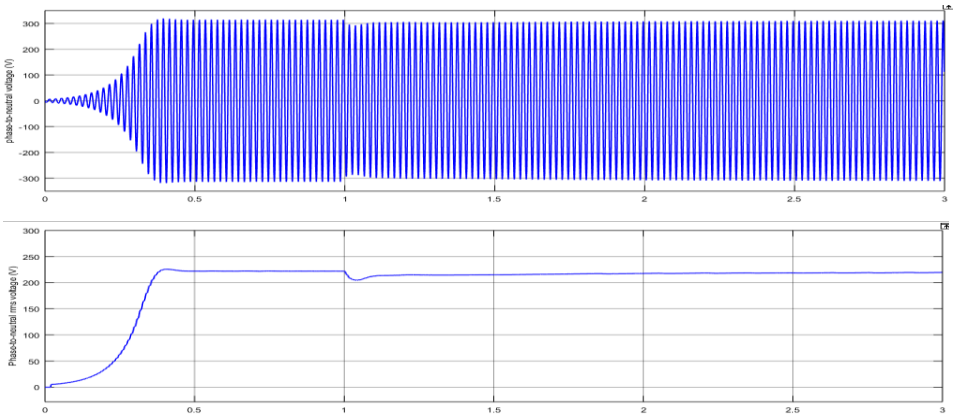

Figure 3-12 Phase-to-neutral and phase-to-neutral rms output voltage. 3rd case.

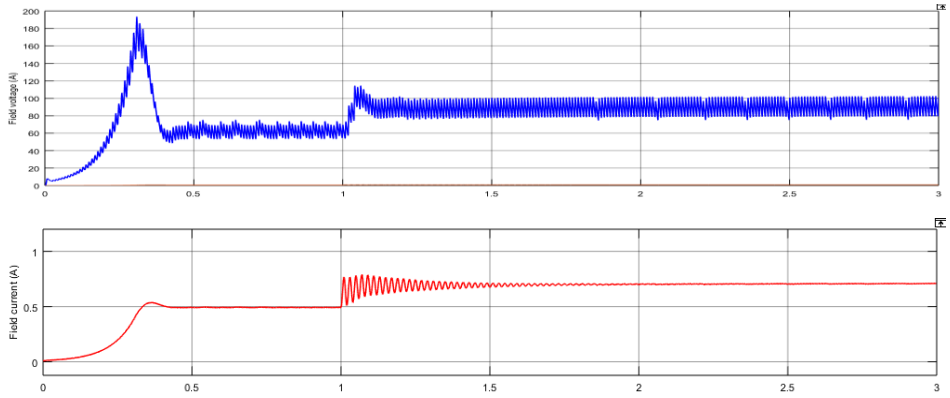

Figure 3-13 Field voltage and field current. 3rd case.

The response of the system when connecting several loads at different times of operation is illustrated in Figure 3.8. As it is remarkable, the AVR tends to correct the effect of connecting the first load, this can be seen in Figure 4.8 (c) where the field current first rises. Not so long, a second load is connected adding influence on the SG. The AVR takes corrective actions again, giving rise to field current again.

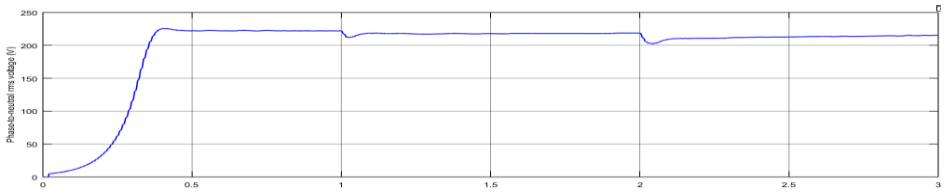

Figure 3-14 Phase-to-neutral rms output voltage. 4th case.

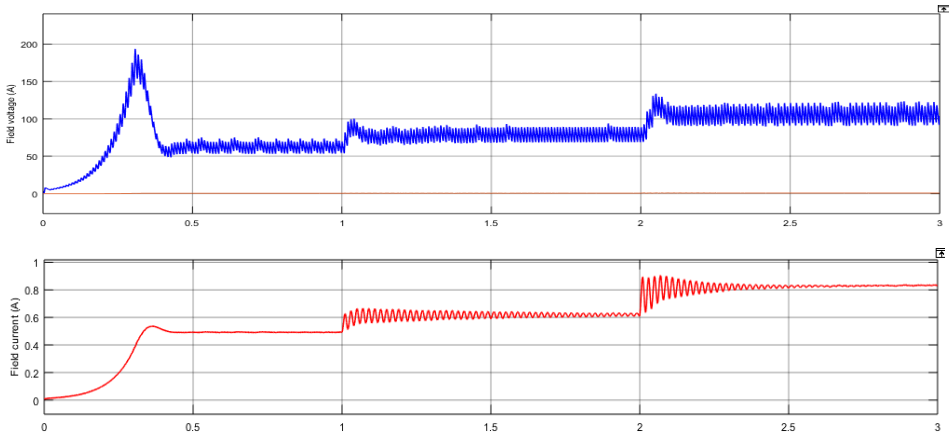

Figure 3-15 Field voltage and field current. 4th case.

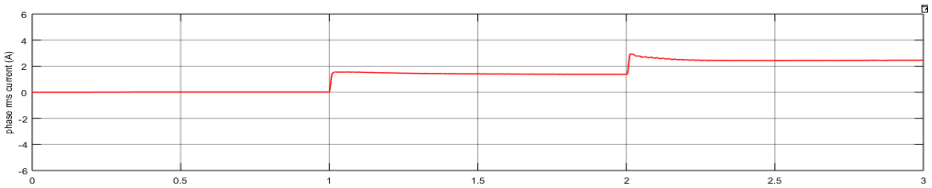

Figure 3-16 Single-phase rms current. 4th case.

CHAPTER 4 : Experimental Hardware Setup

4.1 Firing Circuit Implementation

The previously explained firing circuit was implemented by means of electronic and logic ICs, shown on figure 4.1.

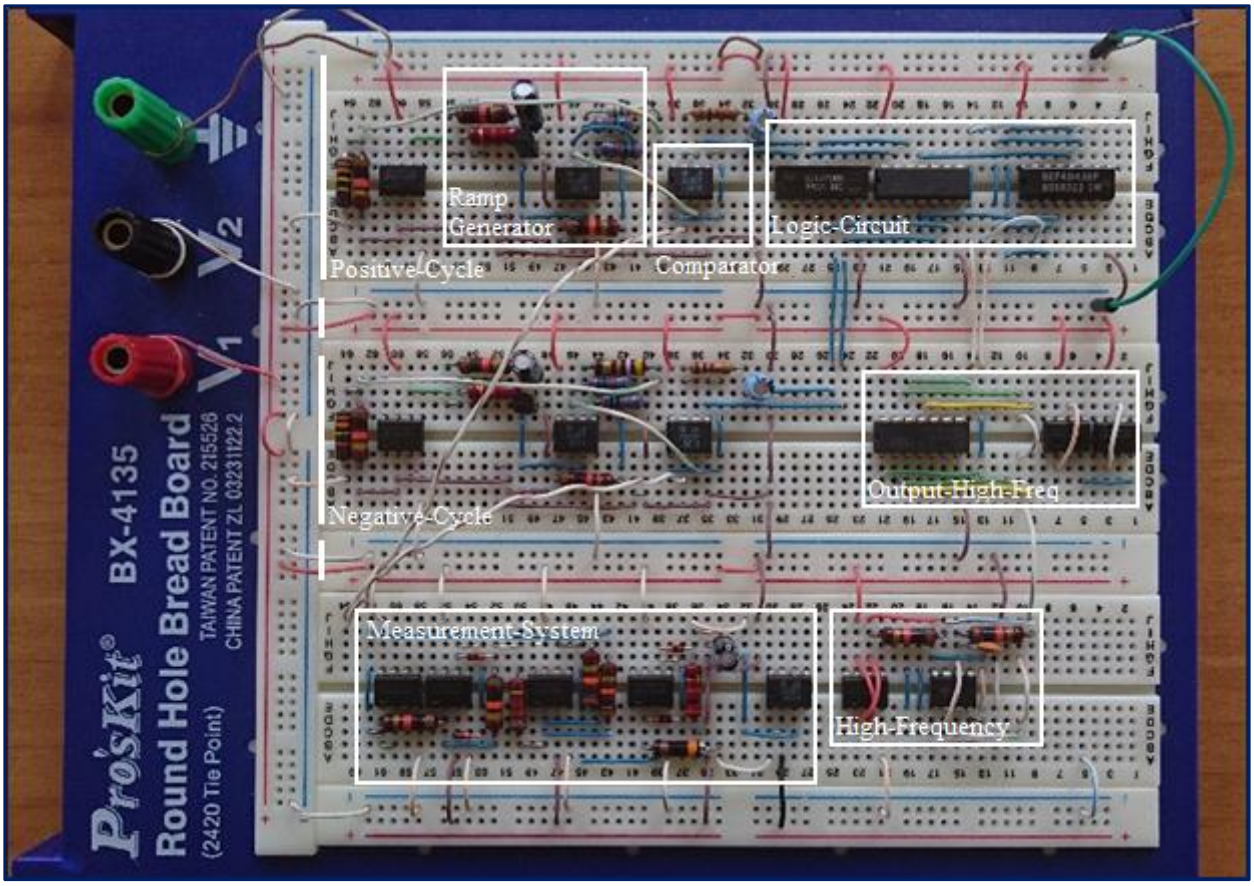

Figure 4-1 Firing Circuit and Measurement system.

The circuit is tested using synchronization transformer 220/17 volts to provide the sinusoidal signal of frequency of 50 Hz. A potentiometer is used to provide a control signal of 4 volts. Thus, the firing angle alpha is $\alpha = 1.196$ rad.

Results are summarized in figure 4.2.

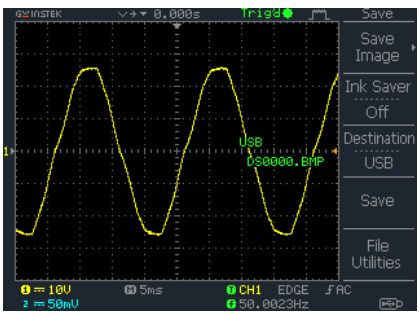

Sinusoidal input signal to the firing circuit of 17 volts rms and frequency of 50 Hz.

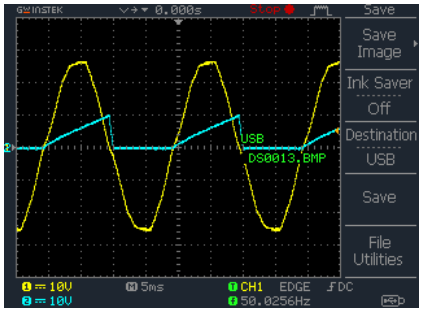

Ramp signal of 10.5 V peak value is generated and is synchronized to the input signal.
(Positive cycle)

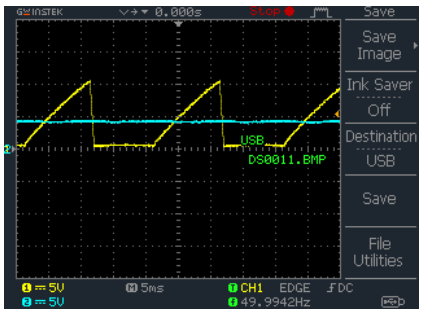

A dc control voltage signal of 4 V is to be compared to the synchronized-ramp signal to generate firing pulses.

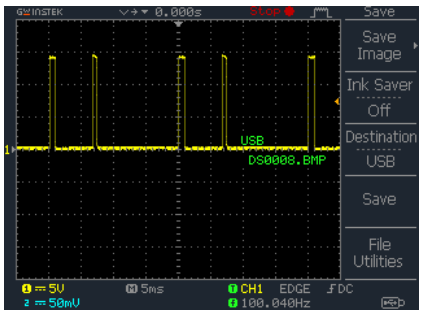

A pulse is generated at each crossing of the control signal and the synchronized-ramp signal.

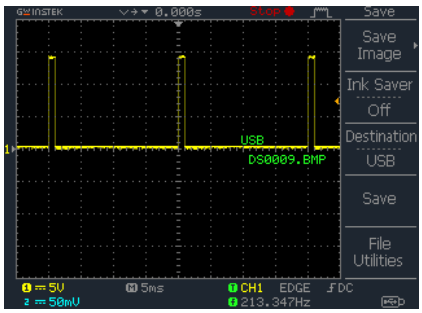

AND logic gate is used to eliminate the second pulse at each period.
(Only the first pulse is needed)

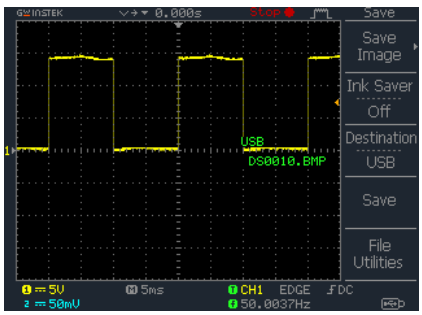

The SR-latch output is square wave of length π.

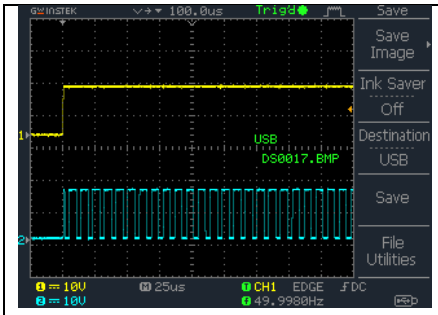

The SR latch output signal is to be multiplied by a high frequency signal generated by 555-timer (about 5KHz and duty cycle of 70%).
The resulting signal is shown in blue.

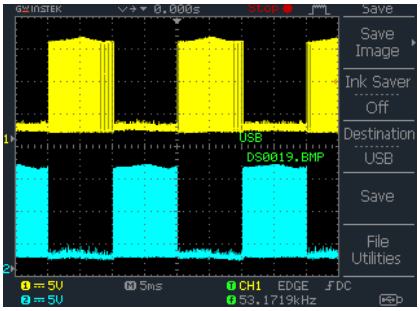

Both output signals of the firing circuit are shown: The yellow signal is for positive cycles and the blue signal is for the negative cycles.

Figure 4-2 Firing circuit test results.

4.2 Programmable Logic Controller

A programmable logic controller (PLC) is a type of digital computer that have an input and output interface, controlled by a simulated program in computer. In this work, Omron CJ1M-CPU 11 PLC is used as controller to implement PID-regulation. CX programmer version 9.5 is used to create the ladder program.

The Omron PLC receives an input signal from the measurement system. Calculations are made in the CPU unit where PID corrective actions take place to generate a dc voltage control signal at the output [15]. The dc voltage control signal is then transferred to the firing circuit to generate firing pulses for the controlled rectifier.

In order to read analog inputs and write analog outputs from-and to- the PLC unit, an analog I/O expansion is needed. For that, the CJ1W-MAD42 module was used, the specifications for this expansion is illustrated (Table 4.1): [16]

Item		
Number of analog inputs	4	
Input signal range	Voltage 1 to 5V 0 to 5V 0 to 10V	Current 4 to 20 mA

	-10 to 10 V	
Maximum rated input	± 15V / ± 30 mA	
Resolution	4000/8000(full scale)	
Converted data	16-bit binary data	
A/D conversion time	1.0 ms/500 µs	
Number of analog outputs	2	
Output signal range	Voltage 1 to 5V 0 to 5V 0 to 10V -10 to 10 V	Current 4 to 20 mA

Table 4-1 Analog I/O module MAD42 specifications.

Figure 4.3 shows the wiring of the module:

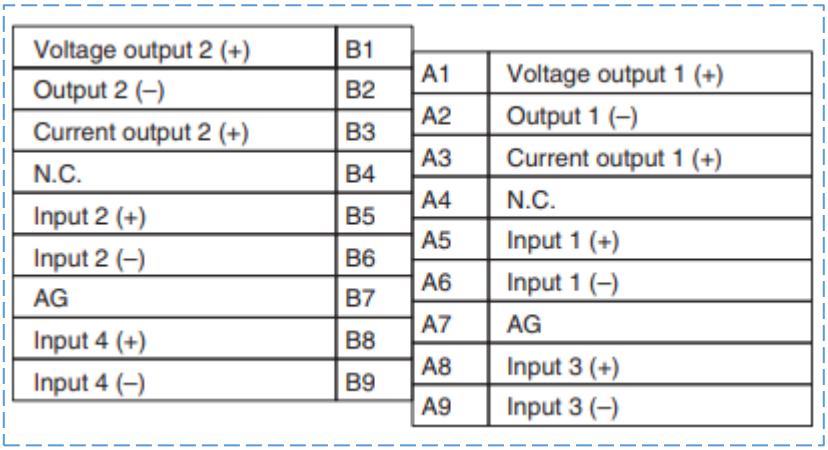

Figure 4-3 Analog I/O module wiring.

After wiring the MAD42 Module, it is necessary to write a ladder program to configure the unit and the data conversion. A special memory is held for the expansion in order to enable the use of the different inputs and outputs. The data conversion is made based on a range code loaded via the ladder program. [16]

In order to implement the PID function, CX-programmer provides a data control instruction block for the PID function: [15]

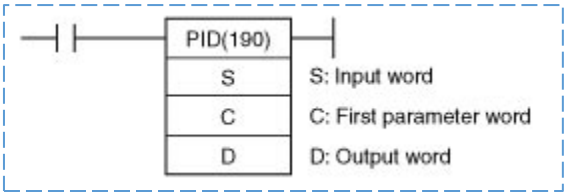

Figure 4-4 PID function block in CX-Programmer.

Where:

S: represents the input word address of the converted analog signal coming from the measurement system (actual value of the terminal voltage).

C: is the first parameter address holding the PID configuration (Set point, proportional gain, integral time, derivative time, sampling period, reverse or forward action, output range and output limitation).

D: represents the output word address holding the manipulated output value, which is then converted from digital to analog and written to the analog output as control signal.

The configuration of the block is done by setting the parameters as follows:

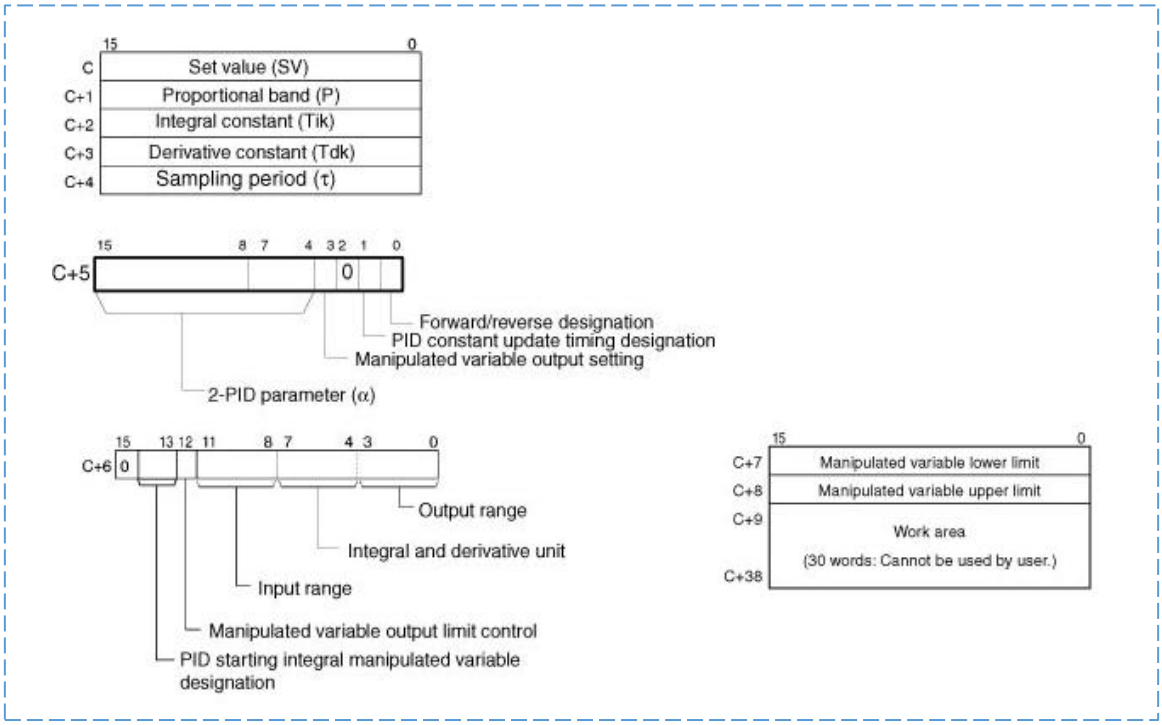

Figure 4-5 PID function block parameters.

The following ladder program is created to implement the PID function. During the first cycle the parameters for the PID block are set.

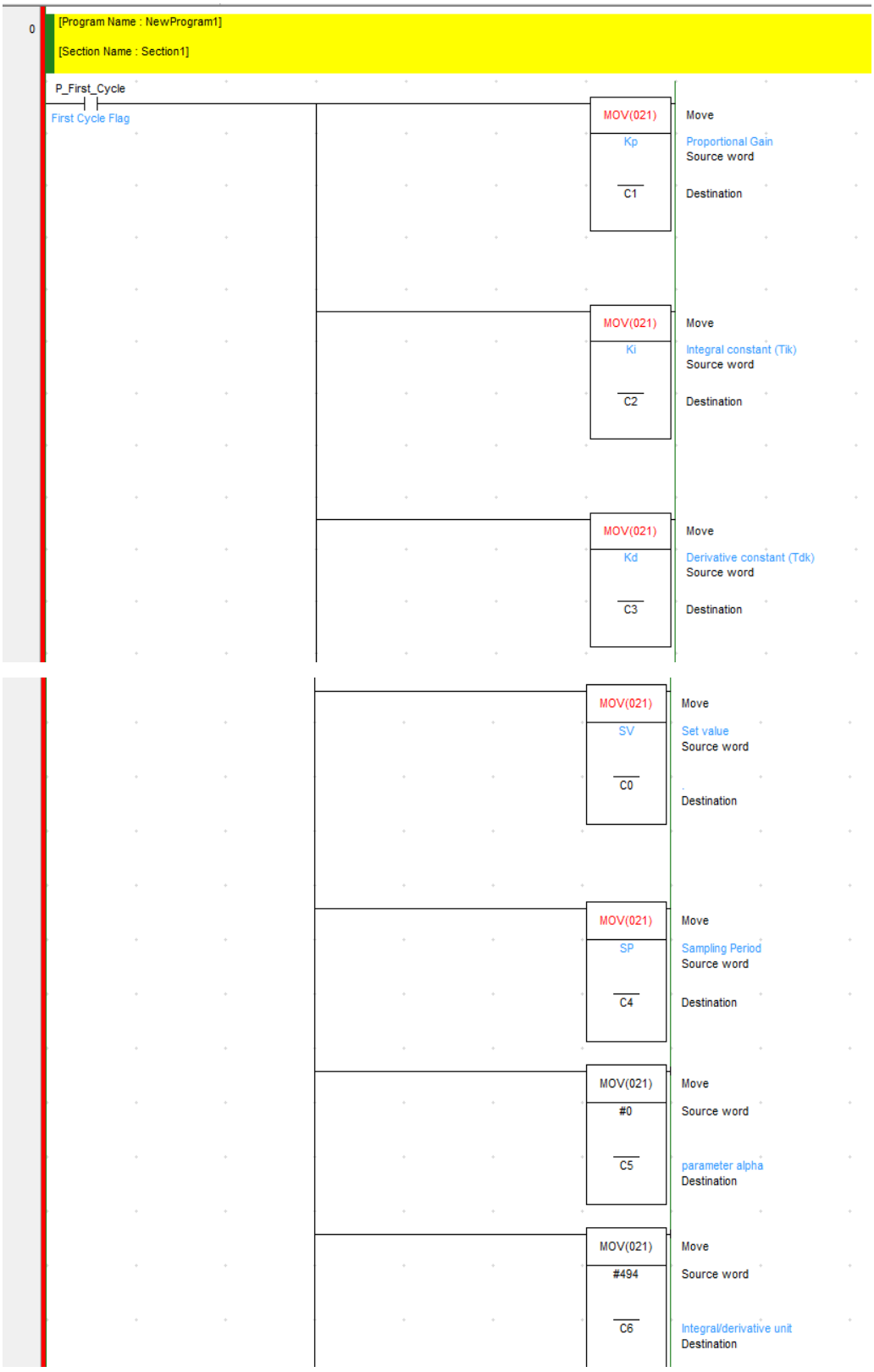
0
[Program Name : NewProgram1]
[Section Name : Section1]
P_First_Cycle
First Cycle Flag
MOV(021)
Kp
C1
Move
Proportional Gain
Source word
Destination
MOV(021)
Ki
C2
Move
Integral constant (Tik)
Source word
Destination
MOV(021)
Kd
C3
Move
Derivative constant (Tdk)
Source word
Destination
MOV(021)
SV
C0
Move
Set value
Source word
Destination
MOV(021)
SP
C4
Move
Sampling Period
Source word
Destination
MOV(021)
#0
C5
Move
Source word
parameter alpha
Destination
MOV(021)
#494
C6
Move
Source word
Integral/derivative unit
Destination

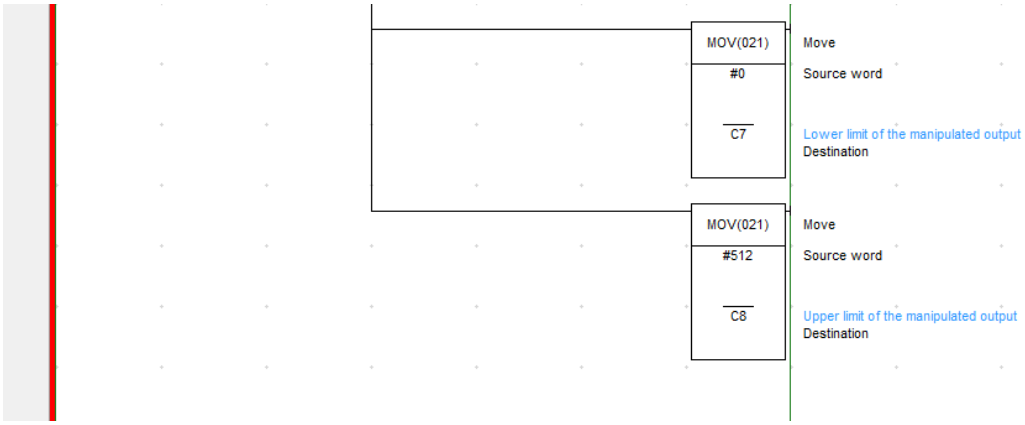

Then the P_on flag (always on) is used to put the PID block on action, read input word (process variable) and write output word (control signal).

GENERAL COCNLUSION

The modeling of the synchronous machine in the natural reference frame as well as in stator reference frame is presented in this work. Identification tests were performed on the laboratory 1.5kVA salient pole SG to extract the machine parameters. Resulting graphs of tests were explained. Validation of the obtained model has been done based on comparison between the graphs obtained by simulation and those obtained experimentally.

The self-excitation system of type ST1A is implemented with an AVR based PI-characteristics. The AVR on the other hand is implemented in Omron PLC. CX-programmer v9.5 was the software tool to write ladder program for the PI-controller as a function block. PI-gains were then set based on two tuning methods: a conventional method where zero/pole cancelation is used and a heuristic algorithm based PSO. The link between the control unit and the power circuit is achieved by a firing card that is designed and implemented based ramp-comparator strategy.

Simulation were made by means of Matlab/Simulink software where the SimPowerSystems library is greatly used. Results of simulation were finally obtained and discussed. Up to this point, every part of the excitation system used works properly and satisfactory.

REFERENCES

[1] Mohamed Labib Awad. "Modeling of Synchronous Machines for System Studies", University Of Toronto, Toronto, Canada, 1999.

[2] P. Kundur. "Power System Stability and Control", New York: McGraw-Hill Inc, 1994.

[3] Ion Boldea. "Synchronous Genrators" -Second edition- Timisoara: CRC Press, 2016.

[4] Daw Ghanim. "Experimental Dtermination of Equivalent Circuit Parameters for a Laboratory Salient-pole Synchrnous Generator", University of Newfoundland, Newfoundland, Canada, 2012.

[5] Abdallah Barakat. "Analysis of synchronous machine modelling for simulation and industrial applications", Article, University of Poitiers, Poitiers, France, 2010.

[6] P.C. Sen, Modern Power Electronics, Wheeler Publishing, 1998.

[7] Wei, and Zheng Xu, Member, IEEE, "Excitation System Parameters Setting for Power System Planning". Power Engineering Society Summer Meeting IEEE 2002.

[8] Tirtharaj Sen, Pijush Kanti Bhattacharjee, Ms. Manjima Bhattacharya. "Design and Implementation of Firing Circuit for Single-Phase Converter", International Journal of Computer and Electrical Engineering, Vol. 3, No. 3, June 2011.

[9] Christian Blum, Daniel Merkle, «Swarm Intelligence: Introduction and Applications», Natural Computing Series, Springer-Verlag, Berlin Heidelberg, 2008.

[10] Kennedy J, Eberhart R (1995) Particle swarm optimization. Proc IEEE Int Conf Neural Netw 4:1942–1948.

[11] Shi Y, Eberhart R (1998) A modified particle swarm optimizer. In: Proceedings of IEEE World Congress on computational intelligence. The 1998 I.E. international conference on evolutionary computation, pp 69–73.

[12] Anthony Carlisle and Gerry Dozier, "An Off-The-Shelf PSO", in Workshop Particle Swarm Optimization, Indianapolis, 2001.

[13] Ajith Abraham, and Amit Konar Swagatam Das. (2008) www.softcomputing.net. [Online]. http://www.softcomputing.net/aciis.pdf

[14] M. Clerc and J. Kennedy (2002). The particle swarm explosion, stability, and convergence in a multidimensional complex space. IEEE Transactions on Evolutionary Computation, 6(1): pp. 58-73.

[15] W228 Omron Programming manual, 2005.

[16] W345–E1–2 Omron Analog I/O unit operational manual, 1999.